UNCLASSIFIED

AD NUMBER
ADB015476
LIMITATION CHANGES

TO:

Approved for public release; distribution is unlimited.

FROM:

Distribution authorized to U.S. Gov't. agencies only; Test and Evaluation; MAY 1976. Other requests shall be referred to Air Force Materials Laboratory, Nonmetallic Materials Division, Composite and Fibrous Materials Branch, AFML/MBC.

AUTHORITY

afwal ltr, 21 sep 1982

THIS PAGE IS UNCLASSIFIED

UNCLASSIFIED

AD B015476
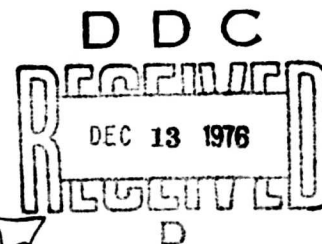
AUTHORITY: AFWAL
ltr, 21 Sep 82

UNCLASSIFIED

ADB015476

GRAPHITE FIBERS FROM PITCH

UNION CARBIDE CORPORATION
CLEVELAND, OHIO

389 450 s/c

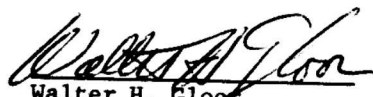SEPTEMBER 1976

D D C
RECEIVED
DEC 13 1976
D

AIR FORCE MATERIALS LABORATORY
AIR FORCE WRIGHT AERONAUTICAL LABORATORIES
AIR FORCE SYSTEMS COMMAND
WRIGHT-PATTERSON AIR FORCE BASE, OHIO 45433

NOTICE

When Government drawings, specifications, or other data are used for any purpose other than in connection with a definitely related Government procurement operation, the United States Government thereby incurs no responsibility nor any obligation whatsoever; and the fact that the Government may have formulated, furnished, or in any way supplied the said drawings, specifications, or other data, is not to be regarded by implication or otherwise as in any manner licensing the holder or any other person or corporation, or conveying any rights or permission to manufacture, use, or sell any patented invention that may in any way be related thereto.

This final report was submitted by Union Carbide Corporation, Cleveland, Ohio under contract F33615-75-C-5109, job order 73200135, with the Air Force Materials Laboratory, Wright-Patterson Air Force Base, Ohio. Walter H. Gloor AFML/MBC was the laboratory project monitor.

This technical report has been reviewed and is approved for publication.

Walter H. Gloor
Project Monitor

For the Director

T. J. REINHART, JR. Chief
Composite & Fibrous Materials Branch
Nonmetallic Materials Division

Copies of this report should not be returned unless return is required by security considerations, contractual obligations, or notice on a specific document.

AIR FORCE - 22 NOVEMBER 76 - 200

REPORT DOCUMENTATION PAGE

READ INSTRUCTIONS
BEFORE COMPLETING FORM

1. REPORT NUMBER	2. GOVT ACCESSION NO.	3. RECIPIENT'S CATALOG NUMBER
AFML-TR-73-147-Pt-4		Final

4. TITLE (and Subtitle)

GRAPHITE FIBERS FROM PITCH.

5. TYPE OF REPORT & PERIOD COVERED
Technical Report. Part IV
April 1975 — May 1976

6. PERFORMING ORG. REPORT NUMBER

7. AUTHOR(s)

R. Didchenko - Principal Investigator

8. CONTRACT OR GRANT NUMBER(s)
F33615 - 75 - C - 5109

9. PERFORMING ORGANIZATION NAME AND ADDRESS
Union Carbide Corporation
P.O. Box 6116
Cleveland, OH 44101

10. PROGRAM ELEMENT, PROJECT, TASK AREA & WORK UNIT NUMBERS
62102F 7320, 73200135

11. CONTROLLING OFFICE NAME AND ADDRESS
DCASR - Cleveland, Federal Office Building
1240 E. 9th Street
Cleveland, OH 44114

12. REPORT DATE
Sep. 1976

13. NUMBER OF PAGES
97

14. MONITORING AGENCY NAME & ADDRESS(if different from Controlling Office)
Air Force Materials Laboratory
AFML/MBC
Wright-Patterson AFB, Ohio 45433

15. SECURITY CLASS. (of this report)
Unclassified

15a. DECLASSIFICATION/DOWNGRADING SCHEDULE
NA

16. DISTRIBUTION STATEMENT (of this Report)

Distribution limited to U.S. Gov't. agencies only;
Test and Evaluation: May 1976. Other requests
for this document must be referred to AFML/MBC
Wright-Patterson, AFB, OH 45433

17. DISTRIBUTION STATEMENT (of the abstract entered in Block 20, if different from Report)

Same as Report

18. SUPPLEMENTARY NOTES

None

19. KEY WORDS (Continue on reverse side if necessary and identify by block number)
CARBON
FIBERS
GRAPHITE
PITCH

20. ABSTRACT (Continue on reverse side if necessary and identify by block number)

Type P fibers are capable of achieving a tensile strength of 4.0 GPa
(approximately 600 Kpsi) with an elongation to break approaching 2.0 per-
cent. However, such properties have been measured only on monofilaments
with $\leq 7.5 \mu m$ diameter, carbonized at $1700°C$ and prepared from a meso-
phase pitch derived from a carefully filtered precursor. The modulus
of the fibers is easily increased by heating to higher temperatures, but the
tensile strength is usually reduced by such treatment.

[handwritten margin note: EQUAL TO THAN OR LESS THAN, MICRO METER]

DD FORM 1473   EDITION OF 1 NOV 65 IS OBSOLETE
1 JAN 73

389450

The tensile strength of the fiber shows a strong dependence on the gauge length, down to about .3 mm. Frequency-of-break analysis revealed a bimodal distribution. Fiber failure below 2.0 GPa (300 Kpsi) is induced by macro-flaws such as foreign particles, voids and surface cracks, all of which were identified by optical and electron microscopy. The wedge-like crack, very common in yarn filaments may cause early fiber failure, particularly when the crack follows a tight spiral along the fiber axis, as it was observed in isolated cases.

The ultimate tensile strength appears to be determined by crystallographic features, such as crystallite size, number of defects, extend of misorientation, as well as by the symmetry of fiber cross section. A cylindrical ▼tree-trunk▲ symmetry always results in higher strength than the radial, ◄wheel-spoke► symmetry.

The electrical properties of the fibers (room temperature resistivity, resistivity ration $\rho(T)/\rho(4.2°K)$, and magnetoresistance) are related to the interlayer spacing (d), the stack height (L_c) and to the degree of three-dimensional graphitic order in the fibers. Fibers with radial symmetry are easier to graphitize than fibers whose cross section exhibits a random structure in polarized light. In general, the three-dimensional order in Type P fibers is much higher than that of PAN-based carbon fibers subjected to the same graphitizing treatment.

Satisfactory interlaminar shear strength can be achieved in Type P fibers by conventional surface treatments. Fibers with cracked filaments result in composites with a relatively low fiber loading, partly because such fibers are poorly collimated. Fibers with round filaments give fiber loadings close to 60 volume percent. Comparison of composite properties, based on a normalized fiber loading, shows that the Young's modulus and the tensile strength of the fibers can be well utilized regardless of whether they contain cracked filaments or not. However, the compressive strength of the composites falls short of expectations, but again the compressive failure may have been induced primarily by inadequate fiber collimation and relatively poor fiber distribution and orientation in the composites.

PREFACE

TABLE OF CONTENTS

PAGE

TABLE OF CONTENTS (Continued)

LIST OF ILLUSTRATIONS

LIST OF ILLUSTRATIONS (Continued)

LIST OF TABLES

LIST OF TABLES (Continued)

SECTION I

INTRODUCTION

The work summarized in this Technical Report is a continuation of the studies conducted under the Contract No. F33615-71-C-1538 and described in Technical Reports AFML TR-73-147, Parts I, II, and III. The goal of the effort was to demonstrate the feasibility of producing high performance carbon/graphitic fibers from mesophase pitch (Type P fibers) in a commercial process.

The desired levels of properties were originally set at 345 GPa (50 Mpsi) for Young's Modulus, 2.75 GPa (400 Kpsi) for tensile strength and ~ 1.3 percent for elongation-to-break, the latter property being paramount. Since initial results indicated the feasibility of achieving much higher levels of strength, the goal for that property was raised to 5.5 GPa (800 Kpsi).

In the pursuit of such high performance levels, it became evident that the macro- and micro-flaws present in Type P fibers had to be identified and related to pitch properties and/or processing parameters. For this reason, much of the work described in this report represents structural studies by means of X-rays, microscopy and electrical measurements. The infusibilization of pitch fibers, the ultimate tensile strength of monofilaments and the performance of Type P fibers in composites are also discussed.

SECTION II

PROCESSING

1. New Thermosetting Atmospheres

Various methods of infusibilizing mesophase pitch fibers were explored during the entire contract effort. In this reporting period, the thermosetting studies were continued mainly under the stimulus of patent disclosures[1,2] which claimed not only to decrease the carbonization time and to increase the carbon yield of ordinary pitch fibers, but also to improve their properties, specifically the degree of graphitic character. Obviously, a process with such advantages should be also very beneficial for the mesophase pitch fibers.

The cited patents describe a two-stage infusibilization in which the first step is treatment of the pitch fibers with conventional gaseous or liquid oxidizing agents. The oxidizing gases, which may be used alone or in mixtures, include ozone, oxygen, air, halogens, sulfur trioxide, and oxides of nitrogen. The liquid oxidizing agents are listed as nitric acid, sulfuric acid, nitrous acid, and acidic dichromate and permanganate solutions. It is recommended that treatment temperatures be above 0°C and below the softening point of the pitch material, preferably between room temperature and 150°C. On a more general basis, the treatment temperature range is listed at 0°C to 400°C with the limitation that the reaction conditions be chosen to avoid significant consumption of the pitch product to be treated or destruction of the matrix molecules. The second stage of the infusibilization technique involves treatment of the oxidized pitch with ammonia or organic amines. Ammonia may be used by itself or in a mixture with air or an inactive gas, such as nitrogen. Temperatures for the ammonia or organic amine treatment are from room temperature to 400°C. The treatment time is governed by the reaction temperature.

It is claimed that the use of the two-stage infusibilization procedure results in high carbon yields because substantially all of the carbon atoms in the pitch remain in the product rather than being partially lost as carbon monoxide or dioxide. The assumed reason for the high carbon yield is that the oxygen or halogen groups introduced during the first step of infusibilization are substituted by a nitrogen-containing group in the second step, with the removal of water or hydrohalogen. When the material is further heated, nitrogen-containing functional groups act as dehydrogenating agents and induce polymerization reactions. The two-stage infusibilization method also affects the structure of the carbonized material. The oxidation of pitch at temperatures less than 300°C produces complex three-dimensional bridging which inhibits the crystal growth of the carbon molecules during the carbonization process. However, the replacement of oxygen functional groups, introduced in the first stage of infusibilization, by nitrogen functional groups in the second stage removes the hindrance to carbon crystal growth and enhances the graphitization. These general concepts were similar to the thinking which governed the development of thermosetting methods used in the present study. It was decided, therefore, to explore whether the specific methods proposed by Araki would result in an improvement of Type P fiber process.

a. Experimental

One group of experiments consisted of oxidizing pitch fibers with nitrogen dioxide, alone or mixed with air, or with ammonia-air mixtures. Gaseous ammonia or methylamine were used in the second stage treatments. The pitch fibers contained 40 percent or 55 percent of pyridine insoluble fraction (P.I.) and produced carbonized filaments with diameters of approximately 12 μm. The infusibilization conditions and properties of the carbonized filaments are given in Tables I and II. The reaction with pure nitrogen dioxide followed by ammonia is a deviation from the patented methods.

In another group of experiments, pitch fibers were allowed to react with chlorine gas or a mixture of chlorine gas with oxygen. The partially infusibilized fibers were then treated with ammonia or methylamine. In addition to the 40 percent P.I. and 55 percent P.I. fibers used in the nitrogen dioxide oxidation experiments, which produced 12 μm diameter carbon filaments, a 55 percent P.I. fiber giving 9.0 μm diameter carbon filaments was used in the chlorination experiments because small diameter fibers are more easily thermoset. The method of treating pitch fibers in chlorine gas at room temperature for 5 minutes, followed by exposure to methylamine at 150°C (6 minutes) and 200°C (5 minutes) was taken from reference 1. Since the chlorine alone was insufficient to render the fibers completely infusible under the conditions used, the method was modified by additional treatment in oxygen for 5 minutes at temperatures ranging from 200°C to 300°C. Secondary treatments included heat treatments in ammonia and methylamine. Reaction conditions and properties of the fibers carbonized at 1700°C are listed in Tables III, IV and V.

The properties of the carbonized filaments subjected to these treatments were generally unsatisfactory. Many of the fiber samples fused during processing so that filaments could not be separated for testing. As can be seen from Tables I through V, only the samples 22D, E and H reached property levels commonly obtained in the past for Type P fibers. The results of experiments with the secondary amine treatment do not seem to bear out the claims that this treatment is capable of increasing the graphitic character. If this were the case, some improvement in Young's modulus would be expected.

b. X-ray Analysis of Fiber Structure

A more definitive proof of improved graphitizability of fibers subjected to the two-stage infusibilization with Lewis acids and bases was sought by means of X-ray analysis. Higher graphitic order is ordinarily reflected in higher values of the layer stack heights L_c. In oriented fibers[3] increased graphitic order usually goes together with improved orientation. The degree of orientation can be measured as the full width at half maximum (FWHM) of the azimuthal densitometer scan of the 002 reflections on a flat plate. The smaller the FWHM (expressed in degrees of angle), the better the orientation.[4] Both these structural parameters are listed in Table VI for series of fibers derived from pitches with 55 percent P.I. The actual thermosetting conditions used for each batch of fibers within this series are listed in Table II.

3

TABLE I

Summary of Processing Conditions and Properties of 12 μm Carbon Fibers
Derived from a Mesophase Pitch with 40% P.I.; Carbonization at 1700°C

Sample	Oxidizing Conditions Gas	Temp., °C	Time, Min.	Amine Treatment Gas	Temp., °C	Time, Min.	Tensile Strength 20 mm	3 mm	Young's Modulus
17A	50% NO$_2$ Air	140	5	NH$_3$	150 200	5 5	Fused	Fused	-
17B	50% NO$_2$ Air	140	5	None	-	-	0.59	0.80	134
17C	NO$_2$	140	5	NH$_3$	150 200	5 5	0.34	1.00	123
17D	50% NO$_2$ Air	140	5	CH$_3$NH$_2$	150 200	5 5	0.66	0.78	163
17E	NO$_2$	140	5	CH$_3$NH$_2$	150 200	5 5	0.78	1.52	119
17F	30% NH$_3$ Air	25-300 at 1°C per min.	-	None	-	-	0.73	1.27	156
17G	Air	25-300 at 1°C per min.	-	None	-	-	1.17	1.17	168
17H	17% NO$_2$ Air	200	30	CH$_3$ NH$_2$	200	30	Fused	Fused	-
17I	17% NO$_2$ Air	200	30	None	-	-	Fused	Fused	-
17J	17% NO$_2$ Air	200	90	None	-	-	Fused	Fused	-
17K	17% NO$_2$ Air	200	30	NH$_3$	200	30	Fused	Fused	-

4

TABLE II

Summary of Processing Conditions and Properties of 12 μm Carbon Fibers
Derived from a Mesophase Pitch with 55% P. I.; Carbonization at 1700°C

| Sample | Oxidizing Conditions | | | Amine Treatment | | | Tensile Strength | | Young's Modulus |
	Gas	Temp., °C	Time, Min.	Gas	Temp., °C	Time, Min.	20 mm	3 mm	
15A	50% NO_2 Air	140	5	NH_3	150 200	5 5	Fused	Fused	-
15B	50% NO_2 Air	140	5	None	-	-	0.71	1.05	133
15C	NO_2	140	5	NH_3	150 200	5 5	0.39	0.32	124
15D	50% NO_2 Air	140	5	$CH_3 NH_2$	150 200	5 5	0.19	0.53	74
15E	NO_2	140	5	$CH_3 NH_2$	150 200	5 5	0.29	0.48	125
15F	30% NH_3	25-300 at 1°C per min.	-	None	-	-	1.12	1.50	129
15G	Air	25-300 at 1°C per min.	-	None	-	-	0.92	1.32	128
15H	17% NO_2 Air	200	30	$CH_3 NH_2$	200	30	0.85	0.99	122
15I	17% NO_2 Air	200	30	None	-	-	0.73	1.12	117
15J	17% NO_2 Air	200	90	None	-	-	0.72	1.51	114
15K	17% NO_2 Air	200	30	NH_3	200	30	Fused	Fused	-

TABLE III

Summary of Processing Conditions and Properties of 12 μm Carbon Fibers
Derived from a Mesophase Pitch with 40% P.I.; Carbonization at 1700°C

| Sample | Oxidizing Conditions | | | Amine Treatment | | | Tensile Strength | | Young's Modulus |
	Gas	Temp., °C	Time, Min.	Gas	Temp., °C	Time, Min.	20 mm	3 mm	
22A	Cl_2	25	5	NH_3	150 / 200	5 / 5	Fused	Fused	-
22B	Cl_2	25	5	$CH_3 NH_2$	150 / 200	5 / 5	Melted	Melted	-
22C	Cl_2	25	5	None	-	-	Fused	Fused	-
22D	Cl_2 / O_2	25 / 300	5 / 5	None	-	-	1.25	1.61	216
22E	Cl_2 / O_2	25 / 300	5 / 5	NH_3	150 / 200	5 / 5	0.82	1.26	207
22F	Cl_2 / O_2	25 / 250	5 / 5	None	-	-	0.40	0.88	141
22G	Cl_2 / O_2	25 / 250	5 / 5	NH_3	150 / 200	5 / 5	-	1.40	-
22H	Cl_2 / O_2	25 / 200	5 / 5	None	-	-	1.44	1.61	221
22I	Cl_2 / O_2	25 / 200	5 / 5	NH_3	150 / 200	5 / 5	0.73	1.01	173

TABLE IV

Summary of Processing Conditions and Properties of 12 μm Carbon Fibers
Derived from a Mesophase Pitch with 55% P. I.; Carbonization at 1700°C

| Sample | Oxidizing Conditions | | | Amine Treatment | | | Young's Strength | | Young's Modulus |
	Gas	Temp., °C	Time, Min.	Gas	Temp., °C	Time, Min.	20 mm	3 mm	
20A	Cl_2	25	5	NH_3	150 200	5 5	Fused	Fused	-
20B	Cl_2	25	5	$CH_3 NH_2$	150 200	5 5	Fused	Fused	-
20C	Cl_2	25	5	None	-	-	0.32	0.48	158
20D	Cl_2 O_2	25 300	5 5	None	-	-	0.62	1.11	136
20E	Cl_2 O_2	25 300	5 5	NH_3	150 200	5 5	0.59	1.14	152
20F	Cl_2 O_2	25 250	5 5	None	-	-	0.78	1.19	157
20G	Cl_2 O_2	25 250	5 5	NH_3	150 200	5 5	0.58	0.84	163
20H	Cl_2 O_2	25 200	5 5	None	-	-	0.43	0.60	151
20I	Cl_2 O_2	25 200	5 5	NH_3	150 200	5 5	0.52	0.74	157

7

TABLE V

Summary of Processing Conditions and Properties of 9 μm Carbon Fibers
Derived from a Mesophase Pitch with 55% P. I. ; Carbonization at 1700° C

| Sample | Oxidizing Conditions | | | Amine Treatment | | | Tensile Strength | | Young's Modulus |
	Gas	Temp., °C	Time, Min.	Gas	Temp., °C	Time, Min.	20 mm	3 mm	
26A	Cl_2	25	5	NH_3	150 200	5 5	Fused	Fused	-
26B	Cl_2	25	5	CH_3NH_2	150 200	5 5	Fused	Fused	-
26C	Cl_2	25	5	None	-	-	Fused	Fused	-
26D	Cl_2 O_2	25 300	5 5	None	-	-	Ignited in O_2		-
26E	Cl_2 O_2	25 300	5 5	NH_3	150 200	5 5	Ignited in O_2		-
26F	Cl_2 O_2	25 250	5 5	None	-	-	1.74	2.38	164
26G	Cl_2 O_2	25 250	5 5	NH_3	150 200	5 5	1.67	2.50	154
26H	Cl_2 O_2	25 200	5 5	None	-	-	-		-
26I	Cl_2 O_2	25 200	5 5	NH_3	150 200	5 5	-		-

8

TABLE VI

Graphite Order Stack Heights (L_c) and Orientation Parameters (FWHM) of 1700°C Fibers as a Function of Thermosetting Mode

Sample	Thermosetting Mode	FWHM ° of Angle	L_c nm	Remarks
15C	Two Stage ($NO_2 - NH_3$)	28	5.66	Filament Deformed
15F	One Stage (NH_3/Air)	27	3.80	Filaments Not Deformed
15H	Two Stage (NO_2/Air–$CH_3 NH_2$)	25	3.96	Filaments Not Deformed
15J	One Stage (NO_2/Air)	28	4.08	Filaments Not Deformed

9

The values of FWHM and of L_c in Table VI are very similar to the values that were commonly obtained in this study for fibers thermoset by other methods and carbonized to 1700°C. Only the L_c value for the batch 15C is significantly larger, but the filaments in this batch were badly deformed as a result of partial melting, i.e., insufficient degree of thermosetting. A better development of graphic order (higher L_c) is undoubtedly the result of carbonization from a partially molten pitch composed of aromatic molecules which have not been highly cross-linked. A direct comparison of well-thermoset fiber batches 15H and 15J shows that the two-stage thermosetting described in the patent literature has no effect on the graphitic character of Type P fibers.

2. Gas Evolution During Processing

In the process of infusibilization, up to 28 weight percent of oxygen can be incorporated in the pitch fibers. This chemically bound oxygen is eliminated during the carbonization as carbon monoxide, dioxide and water. It is important to know when the main gas evolution takes place and to what extent the production of hydrocarbons and volatile tars is suppressed. A study was conducted to follow the evolution of various gases from thermoset fibers during heat treatment up to 1000°C.

The samples were analyzed by means of a Chemical Data Systems Pyroprobe 100 Solids Pyrolyzer which was coupled directly to a Hewlett Packard 7620A gas chromatograph. The analysis of carbon monoxide, carbon dioxide, and water was performed with a thermal conductivity detector. A flame ionization detector was used for the hydrocarbons. The pyrolysis interval (the time in which power is supplied to the heating element) was 10 seconds. The time required to reach any temperature was $\leq$ 0. 5 seconds. Pyrolysis gas from the thermoset fiber was analyzed at 50°C temperature increments from 500°C to 1000°C. The same fiber sample was used for the entire heating series. The chromatographic system was flushed with an inert gas prior to each heating step. The principal gases were carbon dioxide, carbon monoxide and water. Ethane, the sole hydrocarbon gas detected, was present only in amounts below one percent.

The graphical presentation of the analytical data in Figure 1 shows that the amount of carbon dioxide increases with increasing temperatures up to a heat-treatment temperature of 700°C. Between 700° and 850°C, the evolution of carbon dioxide is nearly constant. As the temperature is increased beyond 850°C, the amount of dioxide declines rapidly, probably because of the onset of the $C_8 + CO_2 \rightleftharpoons 2CO$ equilibrium. The amount of carbon monoxide increases with increasing temperatures up to 950°C and then levels off. The most rapid increase in carbon dioxide evolution takes place between 600° and 700°C. This temperature range coincides with the formation of the fine porosity in the fibers. (See Section 3). The water evolution pattern resembles that of carbon dioxide. The amount of water increases with increasing temperatures to 700°C, remains nearly constant to 900°C, and then slowly declines with further heating of the fiber. The content of ethane in the pyrolysis gases was 0. 001 percent at temperatures up to 600°C less than 0. 001 percent at 850°C, and 0. 06 percent at 1000°C.

10
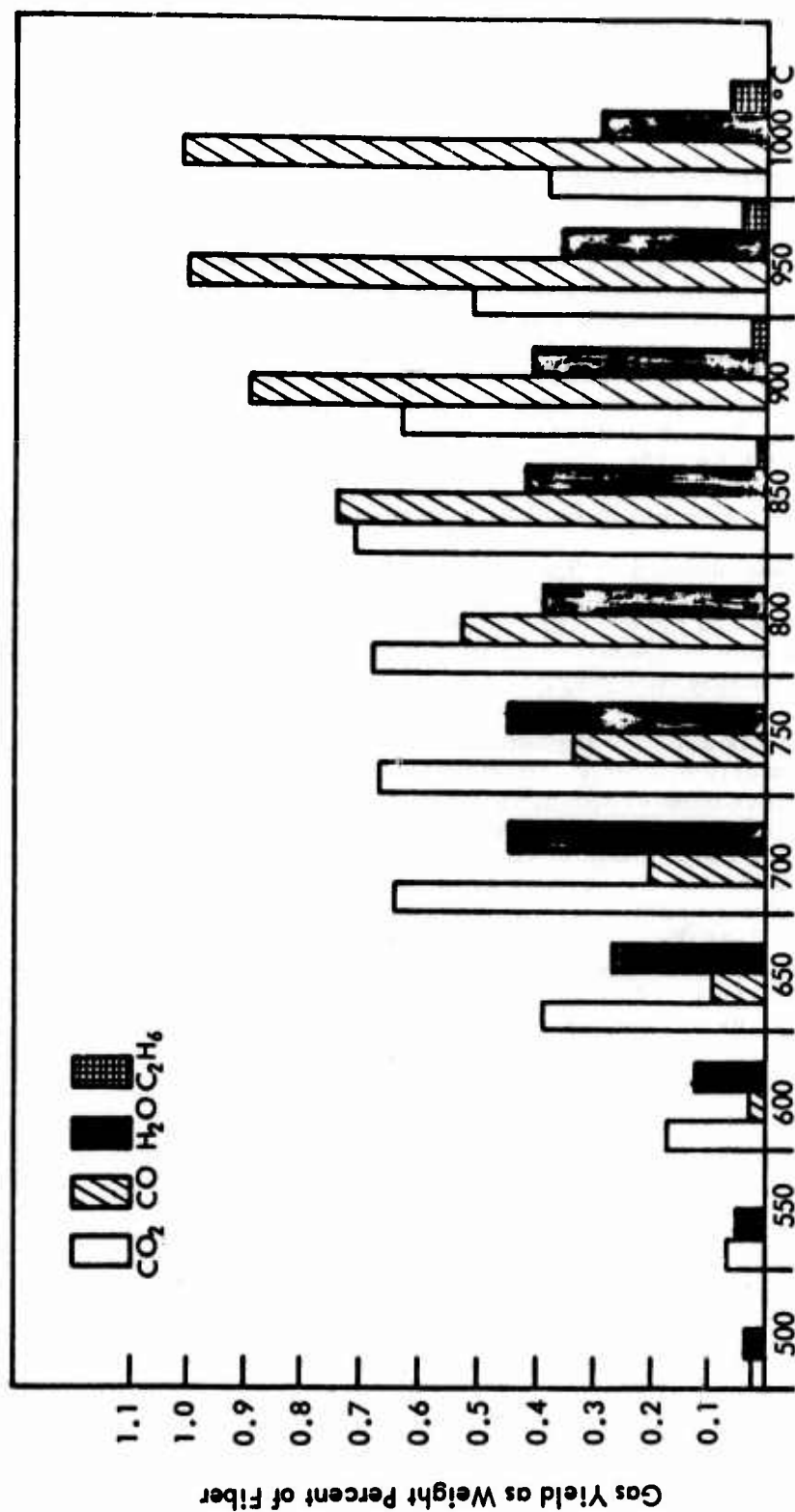
Figure 1. Gas evolution from the stepwise pyrolysis of an infusibilized mesophase pitch fiber.

G760192

11

The gas from the thermoset fiber was also examined in a different mode of pyrolysis. A fresh sample was heated from room temperature to a temperature between 500° and 1000°C. The final temperature was increased each time by 50°C. Figure 2 shows that the amounts of carbon dioxide and water increase with increasing temperature to 800°C, remain nearly constant to 850°C, then increase again with increasing pyrolysis temperature to a maximum at 950°C. Ethane analysis was not carried out during this mode of pyrolyzing, but there is no reason to believe that significant amounts of this gas were formed. Some condensation of heavy tars was observed on the entrance port to the chromatographic column. The amount of these unidentified organic materials was very small.

3. Pore Size Distribution in Partially Carbonized Fibers

It has been noticed in the previous studies of surface areas that the Type P fibers pass through a highly porous stage while being carbonized. The surface area and the development of the porosity was studied as a function of the carbonization temperature using the Digisorb 2500 Automatic Multi-Gas Pore Size and Volume Analyzer.

The surface area for the infusibilized fiber heated at 500°C in an inert atmosphere was only 0.2 m^2/g. However, additional heat treatment at 600°C produced a surface area of 285 m^2/g which was the largest area measured. At this stage, 88 percent of the pores were smaller than 2.0 nm and 11 percent were between 2.0 and 2.5 nm; pressure equilibrium was reached very slowly. After heating to 650°C, the surface area of the fiber was 233 m^2/g with 98.8 percent of the pores below 2.0 nm. Continued heating of the fiber to high temperatures causes the surface area to decrease; fiber heated at 700°C exhibited a surface area of 66 m^2/g, whereas, heating at 900°C resulted in a surface area of only 1.4 m^2/g. Fiber densities ranged from 1.37 to 1.46 Mg/m^3, with the lower value corresponding to fibers with the maximum porosity.

Figure 2. Gas evolution from the pyrolysis of infusibilized mesophase pitch fiber; fresh sample for each temperature.

G760193

13

SECTION III

MONOFILAMENT PROPERTIES

1. Effect of P.I. Content in Mesophase Pitch on Properties of Carbonized Fibers

The severity of the chemical treatments needed to prevent fusing of Type P fibers depends inversely on the pyridine insoluble (P.I.) content of the pitch. Previous attempts to correlate the P.I. content of the pitch with carbonized filament properties were open to doubt because of differences in the filament diameters and in the thermosetting condition of various fiber batches. Furthermore, a statistically meaningful comparison of the available test data was not always possible because of the large variations in the numbers of single filament tests performed on individual fiber samples. These difficulties could be avoided by producing carbonized filament with uniform diameter. Monofilament fiber of about 9 μm diameter, typical of filaments in the yarn, was desirable because it is free from cracks (See Section V) which could complicate measurement of filament diameters. To that end, monofilaments were spun with diameters of 10 to 11 μm from pitches with pyridine insoluble contents of 43, 50 and 56 percent. Filaments from each pyridine insoluble level were infusibilized with four degrees of severity ranging from moderate to relatively severe. The filaments were carbonized in nitrogen at 1700°C. Single filament tensile strengths were measured on 10 filaments of 3.2 mm length (short gauge) and on 5 filaments of 19.8 mm length (long gauge) for each test. Young's moduli were determined from the long gauge tests.

The results in Table VII show that the tensile strengths and moduli of the carbonized monofilaments from each of the three pitches were independent of the severity of the infusibilization treatment. Consequently, all filaments from each pitch can be treated statistically as a part of the same population. The results are shown in Table VIII. Notwithstanding the relatively large standard deviations, the mean values of the tensile strengths, both long and short gauge, indicate a slight trend toward higher tensile strengths for the fibers derived from pitches with higher P.I. content. The modulus values appear to be independent of the precursor, within the range of 43 to 56 percent P.I. content covered in this series of experiments.

2. Filaments from Ultrafiltered Pitch

The removal of finely divided ash particles from a precursor pitch has resulted in a significant improvement in the tensile strength of carbonized monofilaments. The pitch was filtered through a bed of diatomaceous earth supported on a woven metal screen with a nominal opening of 5 μm. This technique is designated as "ultrafiltration" because it removes ash particles which pass through the filters normally used for the removal of solids from precursor pitches. The apparatus used for ultrafiltration is shown in Figure 3. The fiber bed is built in within the metal ring on a stainless steel screen with a nominal opening size of 5 μm. A slurry of "Celite" (diatomaceous earth, marketed by Johns-Mansville Co.) in benzene is used to form the bed by filtering it through the screen. The first filter cake usually shrinks away from the ring upon drying; the crack is filled up by a second filtration. The fragile bed is then reinforced with a coarse screen placed on the top to protect it from disturbance during loading and melting of pitch.

TABLE VII

Carbon Monofilament Properties as a Function of P.I. Content of Mesophase Pitches

Infusibilization Severity Level*	Pyridine Insoluble, %	Long Gauge Tensile		Short Gauge Tensile		Young's Moduli	
		No. of Tests	Avg. GPa	No. of Tests	Avg. GPa	No. of Tests	Avg. GPa
1	43	5	2.21	10	2.09	5	227
1	43	5	1.59	10	2.53	5	190
2	43	5	2.05	10	2.23	5	241
3	43	5	1.87	10	2.36	5	226
4	43	5	1.77	10	1.97	5	225
4	43	5	1.83	10	2.53	5	188
1	50	5	2.57	10	2.51	5	201
2	50	6	1.93	10	2.58	6	198
3	50	7	1.74	10	2.48	7	182
4	50	5	1.49	10	2.09	5	173
1	56	7	2.03	9	2.92	7	193
1	56	6	2.55	10	2.36	6	157
2	56	5	2.45	10	2.39	5	190
3	56	5	2.56	10	2.94	5	200
4	56	6	2.48	10	2.75	6	195
4	56	5	2.01	10	2.25	5	177

* Treatment ranges from moderate (level 1) to severe (level 4)

15

TABLE VIII

Statistical Analysis of Property Data from Table VII

| Property | P.I. 43% | | | P.I. 50% | | | P.I. 56% | | |
	n	$\overline{X}$, GPa	s	n	$\overline{X}$, GPa	s	n	$\overline{X}$, GPa	s
Long Gauge Tensile Strength (GPa)	30	1.89	0.48	23	1.91	0.58	34	2.33	0.67
Short Gauge Tensile Strength (GPa)	60	2.28	0.75	40	2.41	0.60	59	2.61	0.67
Young's Moduli (GPa)	30	216	33	23	188	23	34	186	22
Filament Cross-Section Area (μm^2)	90	53.0	8.8	63	49.2	5.4	93	54.7	7.0

n = number of tests

$\overline{X}$ = mean value

s = standard deviation

16
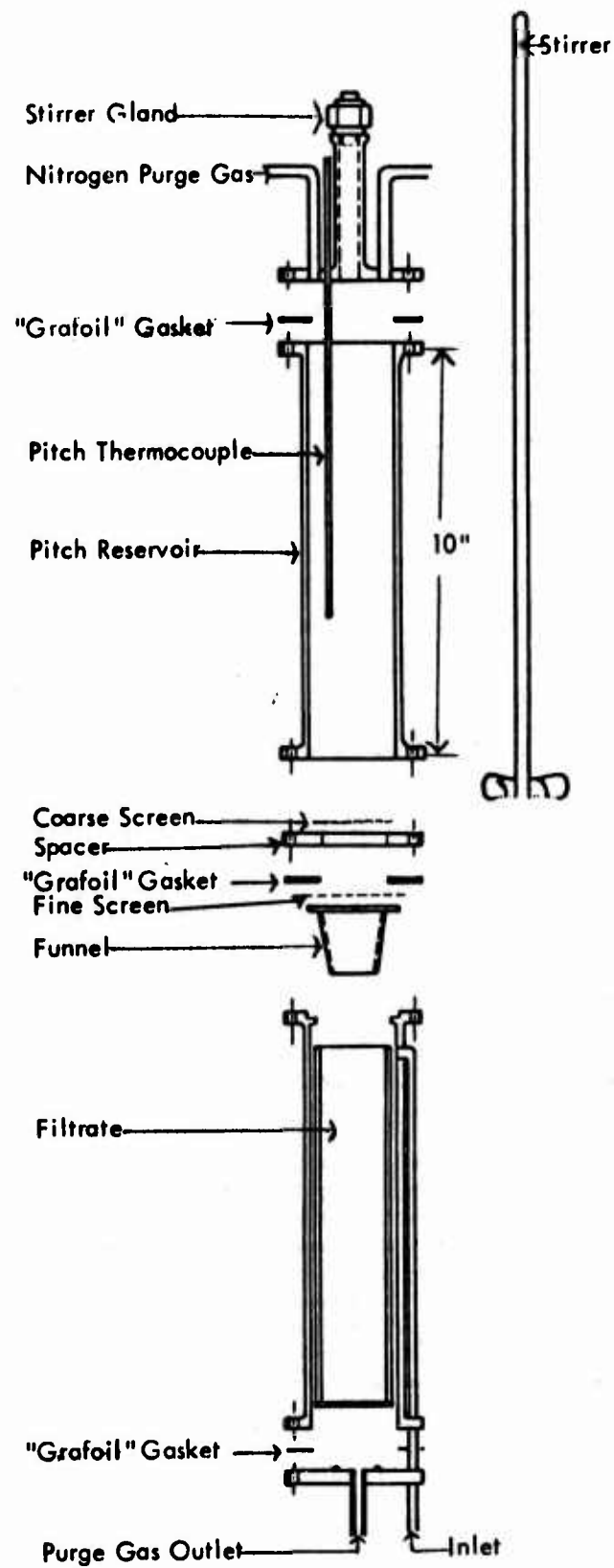
Figure 3. Apparatus for ultrafiltration of precursor pitch.

17

The entire filtering assembly, with about 200 g of crushed precursor pitch in the upper chamber, is placed in a vertical tube furnace and flushed with nitrogen. The pitch is melted and pushed through the filter bed by applying a gas pressure of 10 - 15 psig. The first batch of the pitch is used only to condition the filter and is discarded. The assembly is then ready to filter several batches of precursor pitch which yields a mesophase pitch with a particle content estimated to be about 10 times lower than that obtained from conventionally filtered pitch. The ultrafiltered pitch was used in two extended spinning runs in which average diameters of 10 µm and 8.5 µm were achieved. After heat treatment at 1700°C, the resulting carbon filaments had average diameters of 7.5 µm and 6.5 µm. The infusibilization of the thicker filaments was conducted at four different levels of severity. The thinner filaments received treatment corresponding to the two lowest levels used for the thicker filaments. Table IX lists the properties of the 7.5 µm carbonized filaments. The average 3.2 mm gauge length (short gauge) tensile strengths are very uniform with values ranging from 3.10 GPa (450 Kpsi) to 3.45 GPa (500 Kpsi). The strongest filament tested had a tensile strength of 5.23 GPa (760 Kpsi). Long gauge (19.8 mm gauge length) tensile strengths showed more variation than the short gauge tests, with values ranging from 2.10 GPa (300 Kpsi) to 3.00 GPa (440 Kpsi). Obviously, the filaments were quite strong even at the longer test gauge length.

The filament properties of the eight samples listed in Table IX are very uniform and independent of the severity of the thermosetting treatments. It is justified, therefore, to average all data for any given test and arrive at highly reliable results based on large n. These average results for 7.5 µm filaments are given in Table X along with average values for 6.9 and 6.1 µm diameter filaments which were less extensively tested. The thinner filaments were exceptionally uniform with standard deviations for the cross sectional areas typically 7 to 15 percent within each test sample of 10 filaments. It should be noted that all areas for single filament test were calculated from the average diameter obtained by measuring the highest and the lowest value in a given test sample.

The filaments prepared from the ultrafiltered pitch show little dependence of the short gauge tensile strengths or moduli on the filament diameters. Although the ratio of cross sectional areas of the 7.5 µm and the 6.1 µm diameter filaments was 1.5, the short gauge tensile strengths of the samples differed by only 0.2 GPa. The long gauge tensile strength of the 6.1 µm diameter filaments was about 20 percent higher than strength of the larger diameter filameters, but still was within the range of the standard deviations for these samples (22.2 and 21.4 percent, respectively). No conclusions can be drawn from these data about the relative importance of volume vs. surface flaws in the failure mechanism.

TABLE IX

Properties of 7.5 μm Monofilaments Carbonized at 1700°C

Sample	Young's Modulus		Long Gauge Tensile Strength		Short Gauge Tensile Strength		Diameter	
	GPa	n	GPa	n	GPa	n	μm	n
280-24-13A	221	10	2.90	10	3.19	20	7.5	30
B	251	10	2.49	10	3.08	20	7.5	30
C	254	10	2.12	10	3.20	20	7.7	30
D	280	10	3.01	10	3.15	19	7.5	29
Average of all samples	252 ± 52[1]	40	2.63 ± 0.95	40	3.15 ± 0.73	79	7.55	119
571-20-38A	227	5	2.29	5	3.45	10	7.5	15
B	239	5	2.65	5	3.45	9	7.5	14
C	223	5	2.09	5	3.38	10	7.3	15
D	240	5	2.81	5	3.30	10	7.5	15
Average of all samples	232 ± 17	20	2.46 ± 0.99	20	3.59 ± 0.84	39	7.45	59

[1] All standard deviations are calculated from individual test results.

19

TABLE X

Properties of 1700° C Monofilaments as a Function of Diameters

Diameter, μm	Young's Modulus			Long Gauge Tensile Strength			Short Gauge Tensile Strength		
	$\overline{X}$, GPa	s	n	$\overline{X}$, GPa	s	n	$\overline{X}$, GPa	s	n
7.5	245	44	60	2.57	0.96	60	3.23	0.77	118
6.9	243	18	19	2.53	0.61	19	3.27	0.84	60
6.1	221	18	20	3.11	0.51	20	3.48	0.55	60

3. Tensile Strength as a Function of Gauge Length

The test data listed for the 7.5 μm diameter carbonized filaments in Table IX (571-20-38 filament series) have been extended to provide 40 breaks of randomly picked filaments at each gauge length. The tensile strengths of the filaments are plotted versus test gauge length in Figure 4. The dependence of tensile strength on gauge length resembles the trend observed for glass fibers.[5] The tensile strength increases rapidly as the gauge length decreases to 3 mm. The strength of the 1 mm gauge length is essentially the same as the strength measured at 3 mm gauge length. At gauge lengths longer than 3 mm, the tensile strength is clearly limited by gross structural flaws. In contrast, the filaments shorter than 3 mm seem to reflect the inherent strength of the material which is limited by crystallographic imperfections, i.e., grain boundaries, misoriented domains, etc., rather than by "macroflaws" such as foreign particles, voids, and surface cracks. Further evidence for a dual mechanism of filament failure was obtained from histograms of the frequencies of breaks versus the tensile strength shown in Figure 5. The numbers in the upper right corner of each diagram represent the average values of 9 - 10 breaks of four separate tests at each gauge length. (The averages of these values have been used to construct the plot in Figure 4.) Clearly bimodal distributions appear only at 20 mm and at 3 mm gauge lengths, but if all five histograms are viewed simultaneously, it is apparent that there are two regimes of failure: one at 1.0 - 2.0 GPa, and the other with a maximum frequency of breaks between 3.5 and 4.0 GPa.

All evidence points to a tensile strength of 4.0 GPa (~ 600 Kpsi) as being the maximum strength currently achievable in filaments with diameters between 7 and 8 μm, and with an elastic modulus between 200 and 250 GPa. Not only a very thorough filtration of precursor pitch is necessary to achieve high strength, but also the filaments must be free of macroflaws and have uniform structure. Table XI shows one set of single filament test data from this experimental series, which reflect highly uniform properties.

As mentioned before,[6] the Young's modulus of Type P fibers was very easily increased by raising the temperature of the final heat treatment, but the strength did not rise proportionally with the modulus and, sometimes, was even reduced. This behavior was confirmed again on a batch of filaments prepared from ultrafiltered pitch. After carbonization to 1700 °C these filaments had an average diameter of 6 μm, Young's modulus of 226 GPa, and long and short gauge tensile strength of 3.81 GPa and 3.76 GPa, respectively. After an additional heat treatment at 2300 °C, the Young's modulus increased to 419 GPa (60 Mpsi), but both the long and the short gauge strengths fell to 2.80 and 2.85 GPa, respectively.
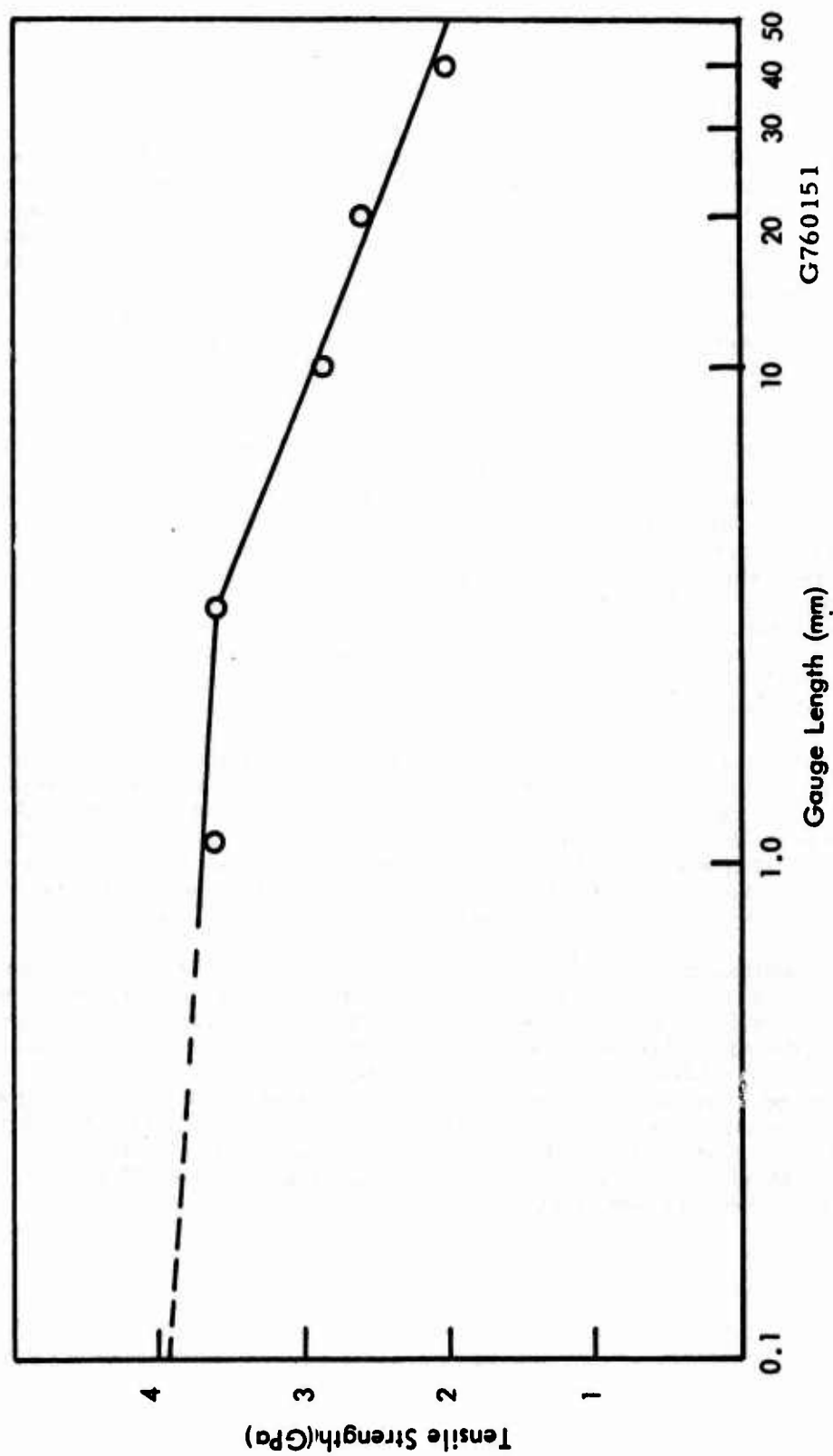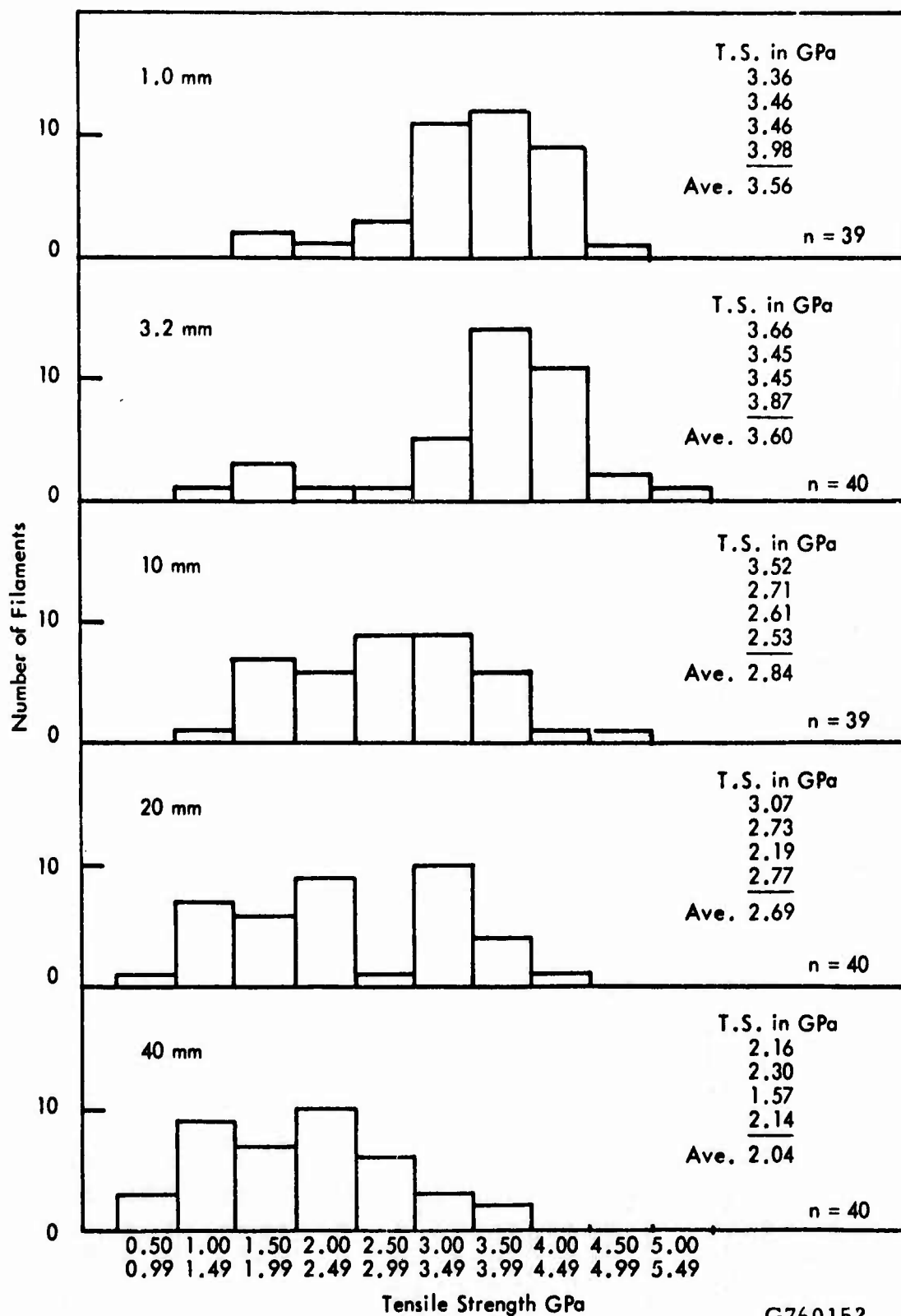
Figure 4. Tensile strength of 7.5 - 8 μm monofilament as a function of gauge length.

G760151

22

Figure 5. Number of filament breaks as a function
of tensile strength at different gauge lengths.

G760152

23

TABLE XI

Printout of Short Gauge Tensile Test

DATE 02-23-76

SUBMITTED BY   J.BARR
CHARGE NUMBER 817-2927
SAMPLE 16022003-1

COMPLIANCE ADJUSTMENT   0.000 NM/GM
MAGNIFICATION/MICROSCOPE CORRECTION FACTOR   0.1318 M/DIV
TO CONVERT GPA TO PSI MULTIPLY GPA NUMBER BY 0.145 X10**6

LENGTH (IN.)	BREAKING FORCE(GM.)	COMPLIANCE (.001 NM/GM.)	C/L (.001/GM.)	TENS. STRENGTH (GPA)	YOUNGS MOD. (GPA)	AREA (SQ. MICROMETERS)
0.320E 01	0.192E 02	0.000E 00	0.000E 00	0.406E 01	0.000E 00	0.479067E 02
0.320E 01	0.178E 02	0.000E 00	0.000E 00	0.381E 01	0.000E 00	0.457205E 02
0.320E 01	0.162E 02	0.000E 00	0.000E 00	0.380E 01	0.000E 00	0.435244E 02
0.320E 01	0.165E 02	0.000E 00	0.000E 00	0.337E 01	0.000E 00	0.479597E 02
0.320E 01	0.178E 02	0.000E 00	0.000E 00	0.349E 01	0.000E 00	0.502655E 02
0.320E 01	0.154E 02	0.000E 00	0.000E 00	0.275E 01	0.000E 00	0.549224E 02
0.320E 01	0.159E 02	0.000E 00	0.000E 00	0.446E 01	0.000E 00	0.415336E 02
0.320E 01	0.168E 02	0.000E 00	0.000E 00	0.385E 01	0.000E 00	0.479674E 02
0.320E 01	0.192E 02	0.000E 00	0.000E 00	0.459E 01	0.000E 00	0.415336E 02
0.320E 01	0.166E 02	0.000E 00	0.000E 00	0.439E 01	0.000E 00	0.415836E 02
0.319E 01	0.160E 02	0.000E 00	0.000E 00	0.387E 01	0.000E 00	0.453200E 02

0.44000E 01 STD. DEV. AREA OR   9.4 PERCENT

0.201E-05 STD. DEV. LENGTH OR   0.0 PER CENT
0.146E 01 STD. DEV. BREAKING FORCE OR   8.0 PER CENT
0.000E 00 STD. DEV. COMPLIANCE OR   0.0 PER CENT
0.000E 00 STD. DEV. COMPLIANCE/LENGTH OR   0.0 PER CENT

0.469E 01 MAX. TENSILE STRENGTH (GPA)
0.275E 01 MIN. TENSILE STRENGTH (GPA)
0.577E 00 STD. DEV. TENSILE STRENGTH OR   14.9 PER CENT

0.000E 00 MAX. YOUNGS MODULUS (GPA)
0.000E 00 MIN. YOUNGS MODULUS (GPA)
0.000E 00 STD. DEV. YOUNGS MODULUS OR   0.0 PER CENT

SECTION IV

ELECTRONIC PROPERTIES OF TYPE P FIBERS

Several investigators have studied the electronic properties of carbon fibers based on textile precursors. Most of these studies have been limited in scope and of relatively little use in characterizing the fibers. A fairly complete study of PAN-based carbon fibers was conducted by Robson et al.,[7] who established a correlation between various electrical properties and the degree of graphitization and preferred orientation of the fibers. These results suggested the possibility of using the electronic properties as a means of studying the structure of fibers.

The present study was motivated by a need to better understand the effect of structure on the mechanical properties of Type P fibers. Since it has not been previously demonstrated what specific structural features place an ultimate limit on mechanical performance of the fibers, it was decided to study the electronic properties of the fibers as a function of processing temperature in order to correlate electronic, structural and mechanical properties.

1. Experimental

a. Sample Preparation

Two batches of pitch fibers were selected, one containing filaments with radial, cracked structure and one having predominantly random structure, (but containing also about 30% radial cracked fibers). These represent variations typically encountered from one pitch lot to another. Each batch of raw fibers was thermoset in each of two different ways, a one-stage process and a two-stage process, so that the effect of thermosetting could be studied. Each of the four resulting fiber samples was then processed at each of the following heat-treatment temperatures (HTT's): 500°C, 1000°C, 1700°C, 2000°C, 2500°C, 3000°C. The heat treatments at 1700° and below were done continuously. Those at 2000° and above were performed on short segments in a graphite capsule in a tube furnace.

b. Measurement Techniques

Resistivity and magnetoresistance measurements were made on single filaments using a four-probe technique. Approximately 0.5 cm lengths of filaments were mounted on 0.001 inch diameter copper wires using Dupont silver preparation 7941 for electrical contact to the sample. The wires were cemented to an insulated copper sample mount having four terminal posts to which the wires were attached (See Figure 6). The mounts were glued to a copper mounting block on the cryostat with GE7031 varnish to provide good thermal contact and were held in position mechanically with spring clips. Leads permanently mounted in the cryostat were attached to the terminal posts on the sample mounts. Up to six samples could be mounted and studied simultaneously. This mounting technique was used in order to minimize strains on the samples. The cryostat used for these measurements was an Air Products and Chemicals Helitran® liquid helium cooled system with an automatic temperature controller.
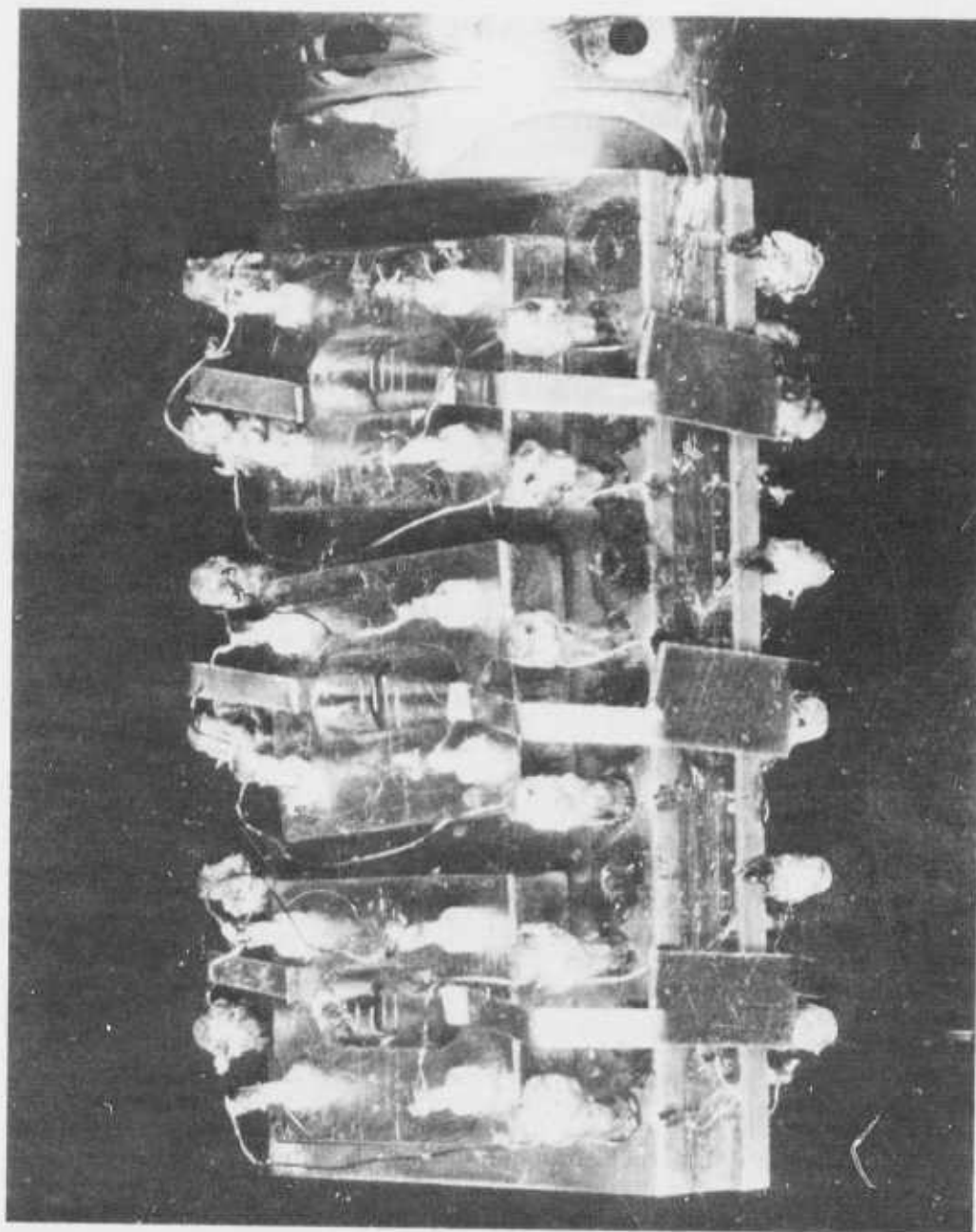
P760098

Figure 6. Sample mount for electrical measurements.

The temperature could be varied continuously over the range from 4.2 °K to 300 °K. The cryostat was placed between the poles of a 12 inch Varian electro-magnet capable of fields up to 14 KG. The sample axis could be aligned parallel or perpendicular to the field by rotating the entire cryostat. The field strength could be swept electronically from maximum to zero in one continuous sweep.

Both DC and AC methods were used for measuring the resistance. The DC method, which was faster but somewhat less accurate, was used during temperature dependence runs where many measurements had to be made in a limited time. A current (usually 10 μA) was passed through the sample using two of the leads and the voltage was measured across the other two leads. Effects of thermal voltages were eliminated by reversing the polarity and averaging the two values. The AC method was used for higher precision, for resistivity ratio and magnetoresistance measurements. A Kelvin bridge arrangement was used with a General Radio decade resistance network with 0.01 ohm resolution used to balance the output. The difference in signals from the decade resistance and the sample was detected using an Ithaco 391A lock-in amplifier. For magnetoresistance measurements, the output from the lock-in amplifier could be used directly as a measure of the change in resistance with magnetic field, sample orientation, etc.

The structures classified as random or radial (See Section V), and the cross sectional area of each filament studied were determined by standard optical microscopy techniques. The samples were potted in epoxy before removal from the mounts. The fiber cross sections were photographed at 2000X and the areas determined by planimetry on the photomicrographs. The length of the sample between the inner pair of leads was measured micro-scopically with a calibrated reticle prior to potting. The length and area were used for determination of the absolute resistivity.

Preferred orientation and crystallite size were measured by X-ray diffraction using a flat-plate technique. The crystallite size (L_c) was estimated from the thickness of the (002) diffraction arc and the preferred orientation was determined from the full width at half maximum (FWHM) of the length of the (002) arc.[4] The d-spacing was measured from the (002), (004) and (006) lines using a cylindrical camera. The degree of 3-dimensional order was estimated by studying the (112) and (101) lines relative to the (110) and (100) lines, respectively, in a powder diffractometer scan.

The tensile strength and Young's modulus of single filaments were measured by the standard methods using a 19.8 mm gauge length and averaging ten breaks for each sample.

2. Results of Electrical Measurements

The resistivity as a function of temperature is shown in Figure 7 for representative fiber samples at various HTT's. The resistivities of fibers heat treated at or below 500° C were too high to measure. The resistivity decreases with increasing HTT. At a given HTT, the resistivity always decreases with increasing temperature, but the precise temperature depen-dence varies markedly from one HTT to another.
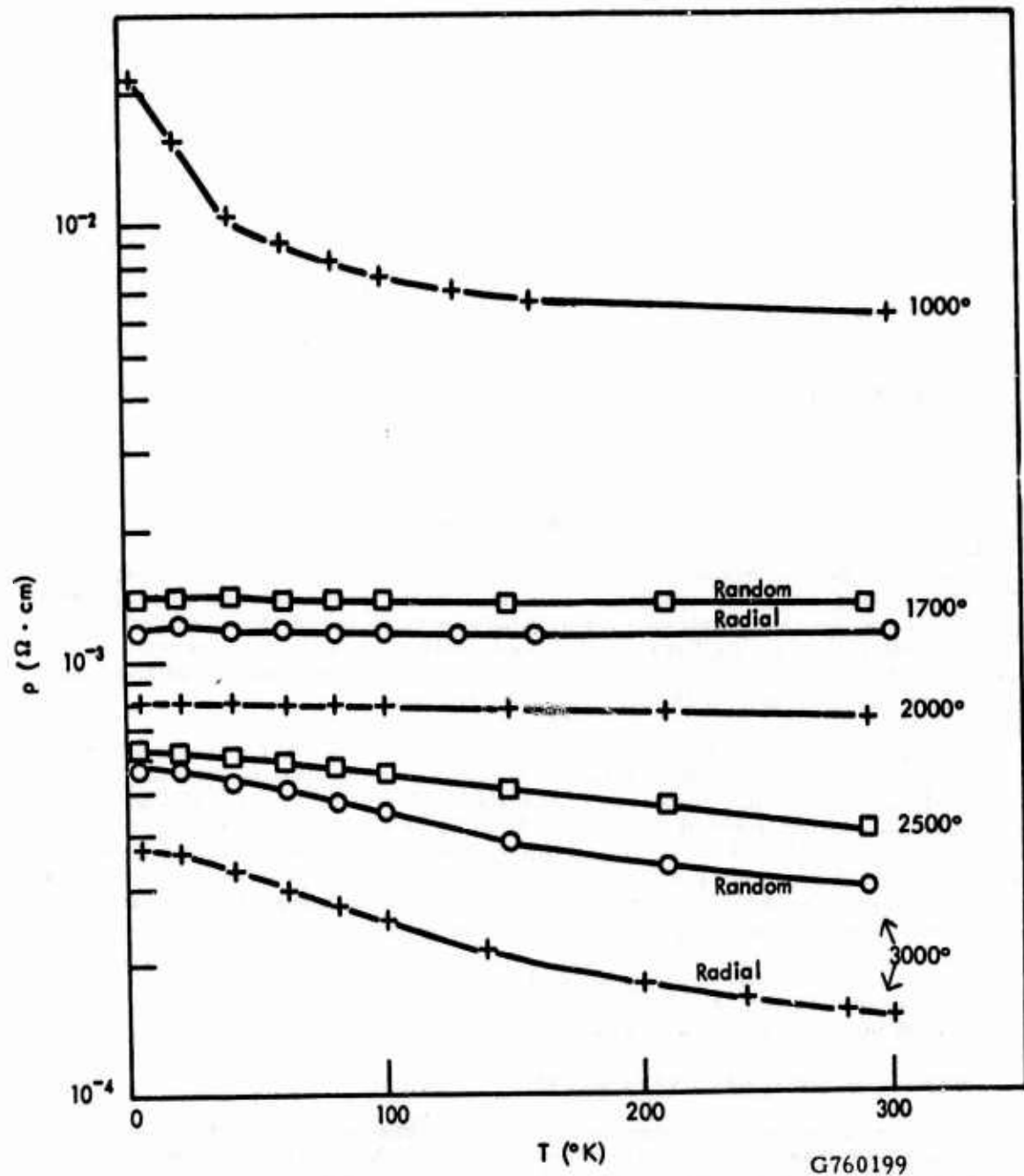
27

Figure 7.   Resistivity as a function of temperature of Type P fibers
with different structures, subjected to several high tem-
perature treatments.

28

The resistivity ratio ρ (4.2° K) /ρ (300° K) decreases from 3.4 at 1000° to 1.08 at 1700°C, then increases to 2.4 at 3000°. Clearly, in the two temperature ranges above and below 1700°C, different changes are taking place in the electronic structure of the fibers. Presumably, the semiconducting energy gap present in the low-HTT material closes around 1700°C. Above this HTT, the structure becomes more and more graphitic and shows a dependence of the number of carriers on temperature similar to that observed in graphite.

The effect of fiber structure on the resistivity is shown also in Figure 7. In fibers heated to 1700°C, there is a small difference in resistivity between radial cracked and random structure fibers, with the radial fibers having the lower resistivity. This difference persists and increases with increasing HTT (the different curves for 2000°C and 2500°C are not shown for clarity) until there is nearly a factor of two differences in the resistivities at 3000°C HTT. This result implies that the radial structure fibers are capable of more complete graphitization than the random fibers.

A similar finding is illustrated in Figure 8 where the temperature dependences of the resistivity ratio $\rho(T)/\rho(4.2°K)$ of three fibers are shown. All of these fibers were simultaneously heat treated to 3000°C to assure identical processing. The fiber with strongly radial cracked structure shows a stronger temperature dependence than the fiber with random structure. The plot for a fiber with weakly radial cracked structure (narrow crack) lies between the other two. These results again imply that the random fiber is less graphitic than the radial fiber.

The magnetoresistance, expressed as the percent change in resistivity as a function of magnetic field, is shown in Figures 9 and 10 for orientation of the field parallel and perpendicular to the fiber's axis, respectively. All measurements were made at 4.2°K. After HTT at 1000°C, the transverse magnetoresistance $MR_\perp$ is small and positive. As HTT is increased, $MR_\perp$ becomes negative and increases in magnitude until HTT reaches the 2500°C range. Above this point, the magnetoresistance becomes positive at high fields and by 3000°C is positive even for low field strengths. The longitudinal components $MR_\parallel$ is unmeasurably small for 1000° HTT, grows steadily more negative (but stays small relative to MR) as HTT increases, and finally becomes slightly positive at high fields for 3000°C HTT, but remains negative at lower fields. As with the resistivity, differences due to fiber structure appear at HTT above 2000°C. The radial fibers have a larger positive magnetoresistance at 3000°C, again indicating more nearly graphitic behavior.

The relationship between resistivity, magnetoresistance and degree of graphitization is illustrated more clearly in Figure 11 which shows the transverse magnetoresistance at 4.2°K in a field of 14 KG plotted against the resistivity ratio $\rho(300°K)/\rho(4.2°K)$. All samples examined in this project had properties lying precisely on the same curve. The different parts of the curve correspond to different degrees of graphitization and, therefore, only approximately to the HTT as indicated.

29
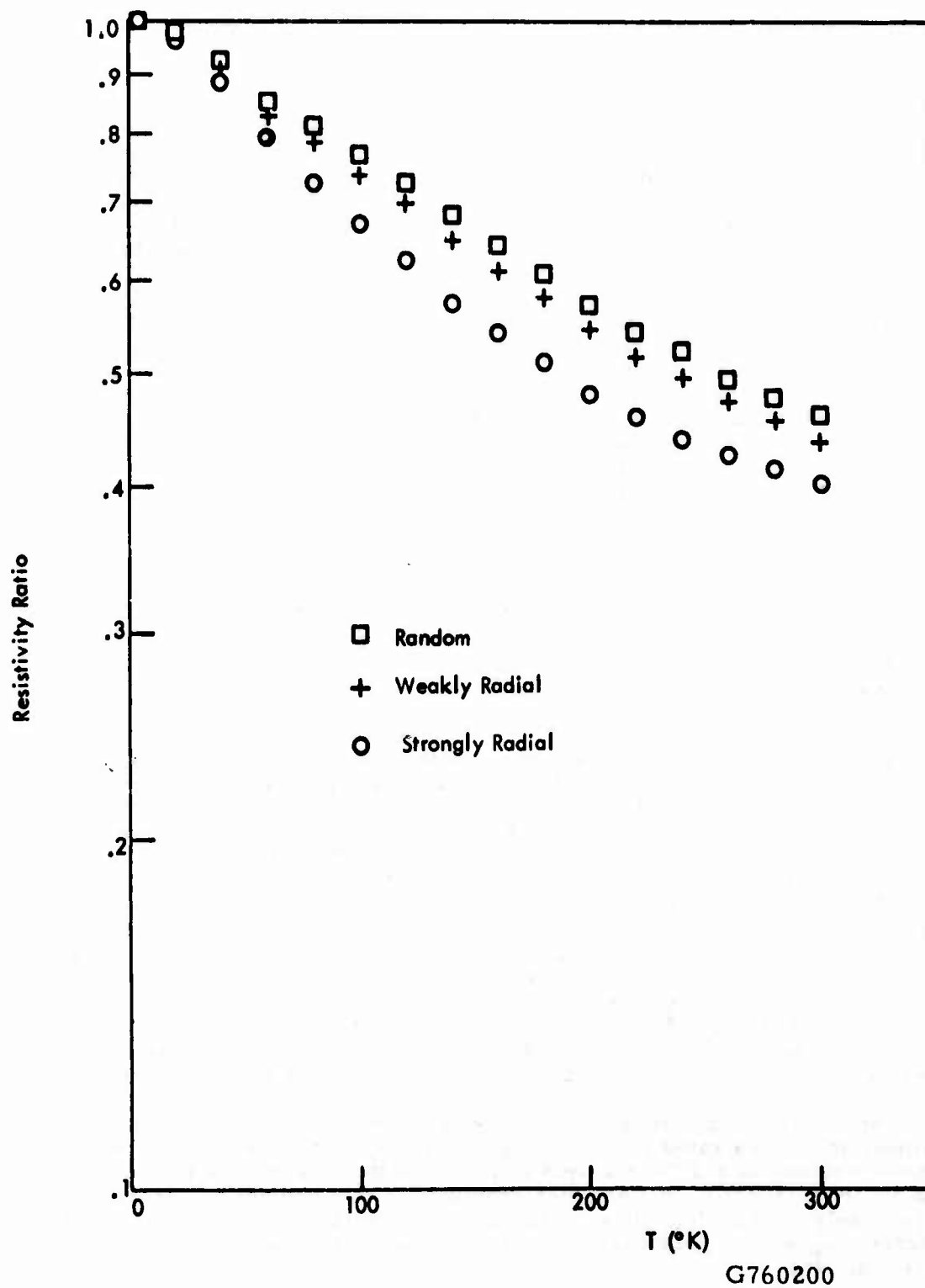
Figure 8. Resistivity ratio $\rho(T)/\rho(4.2°K)$ as a function of temperature for 3000°C heat-treated Type P fibers with three different structures.

G760200

30
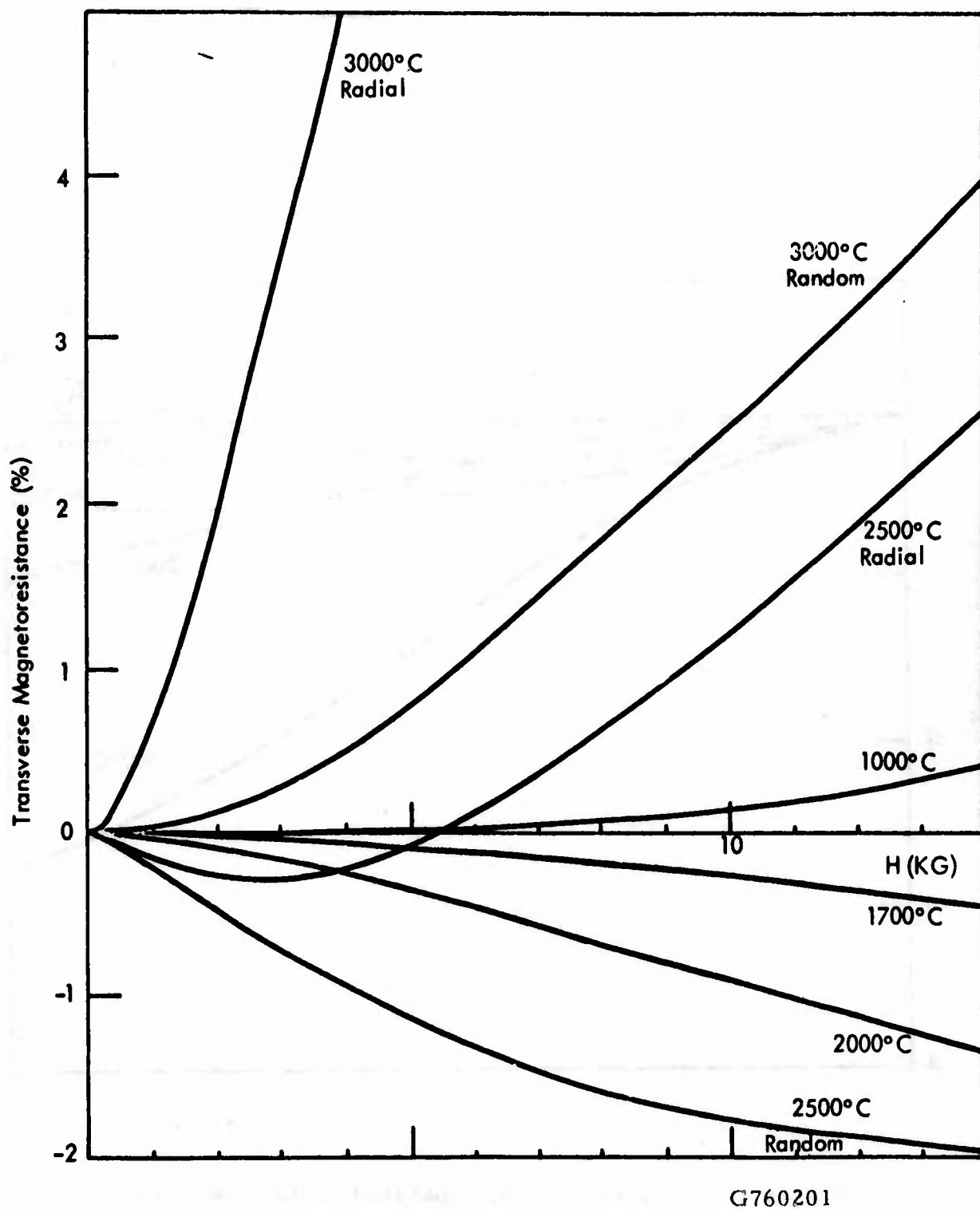
Figure 9. Magnetoresistance perpendicular to the axis of
Type P fibers with different structures and
thermal history.

Figure 10. Magnetoresistance parallel to the axis of Type P
fibers with different structures and thermal history.

G760197

G760128

Figure 11. Plot of the transverse magnetoresistance
versus the resistivity ratio.

33

3. X-ray Results

The preferred orientation of the crystallites in the fibers is shown in Figure 12, where the FWHM of the length of the (002) arc is plotted against HTT for each of the fiber series. Experimentally significant differences are evident for HTT of 1700°C, but above this HTT the dif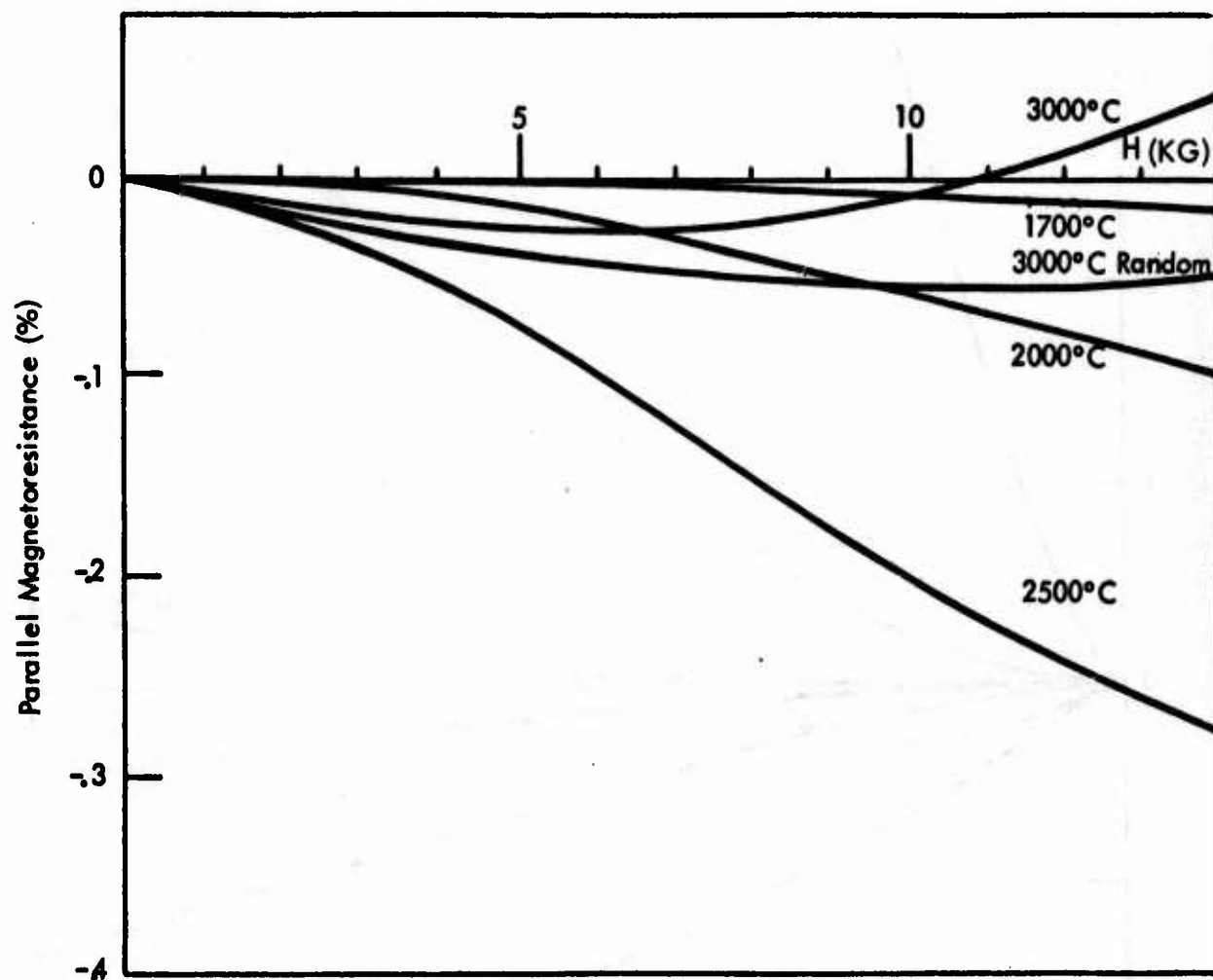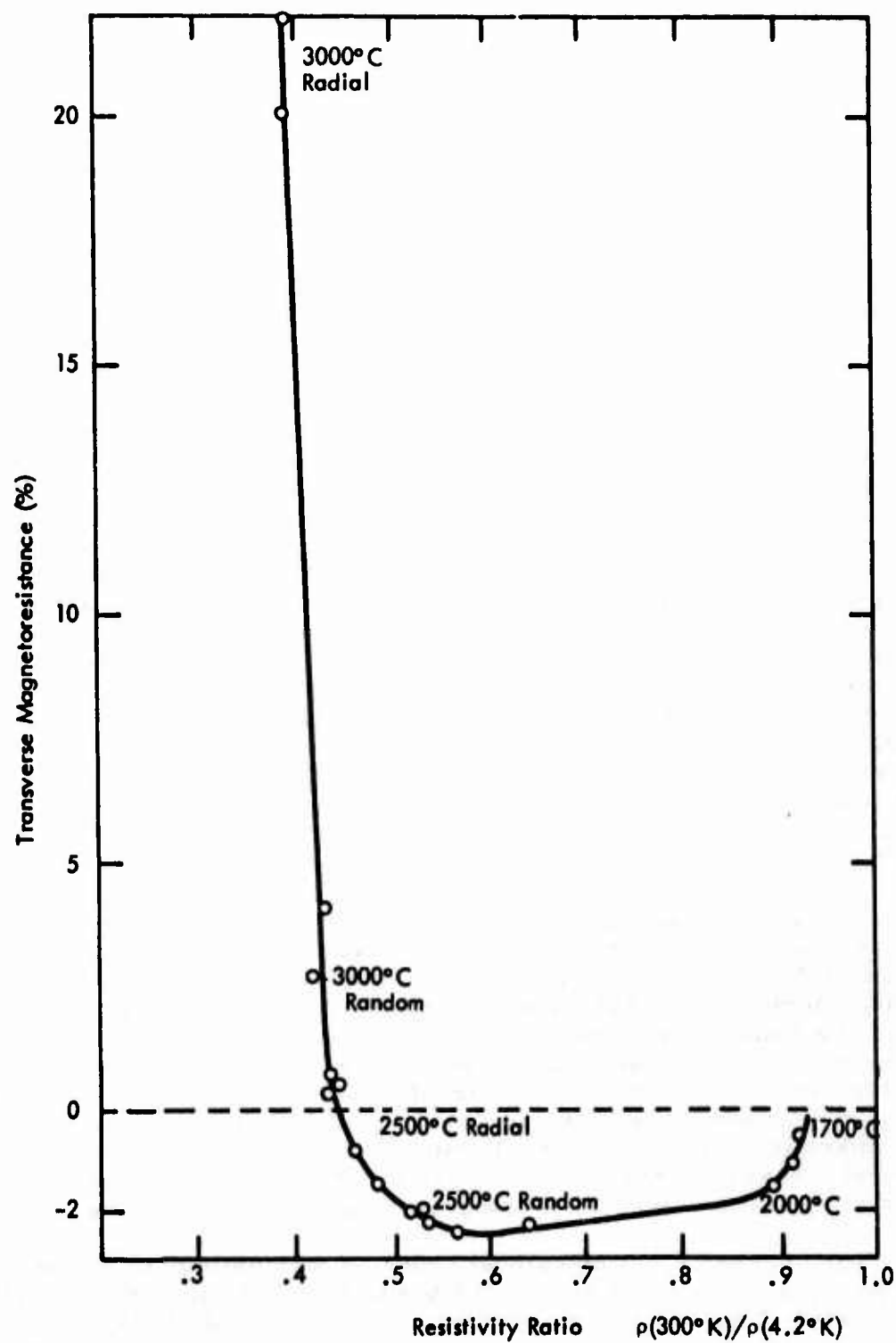ferences are not significant. The random structure fibers are better oriented at first. Their orientation becomes worse on heating above 750°C, but improves again and exceeds that of radial fibers after HTT above 2000°C.

The development of crystallite size is shown in Figure 13. For HTT $\leq$ 1700°C, the L_c values were determined from the (002) peak width using a flat-plate technique. Above 1700°C, HTT, a powder diffractometer was used to measure the (002) and (004) peak widths to obtain L_c values corrected for strain broadening. The uncorrected diffractometer results at 1700°C were in satisfactory agreement with the flat-plate results, but must be considered as lower limits to the true values of L_c and should not be taken too literally. The crystallite size actually decreases at low HTT's, but then increases rapidly from 1000°C to 2500°C. The radial cracked fibers reach a larger value of L_c than the random structure fibers although the differences are insignificant below 1700°C HTT. This result is in good agreement with the findings, based on resistivity and magnetoresistance data, that the random fibers treated to 3000° become no more graphitic than the radial fibers treated at 2500°. This is shown more clearly in Figure 14 where L_c is plotted as a function of the resistivity ratio, a parameter closely related to the degree of graphitization as shown above. All of the fiber series now lie on the same curve. The points for the radial cracked fibers treated at 2500°C are further along the curve than the points for the random fibers treated at 3000°C.

Further corroboration of this result is found in the dependence of d-spacing on HTT. Figure 15 plots the d-spacing against resistivity ratio for HTT of 2500°C (upper points) and of 3000°C (lower points) for each of the four fiber series. The relationship between d-spacing and graphitization is clear. The radial fibers reach a higher degree of graphitization at 2500°C than the random fibers at 3000°. This figure also suggests that the one-stage thermoset fibers have a smaller d-spacing at a given HTT than the corresponding two-stage thermoset fibers. It is not clear why this should be so, as there is no evidence for a greater degree of graphitization from the electrical measurements. Lattice spacings smaller than those shown in Figure 15 can be obtained by prolonging the graphitization time.

The degree of 3-dimensional ordering was estimated by comparing the intensities of the (101) and (112) lines to those of the (100) and (110) lines, respectively. The results indicate that radial cracked fibers show a greater degree of 3-dimensionality than random fibers both at 3000°C and at 2500°C. Again, the radial 2500°C fibers were better ordered than the random 3000° fibers. Below 2500°C, the 3-dimensional lines were too weak to measure. No consistent differences were observed between fibers thermoset in different ways.

34
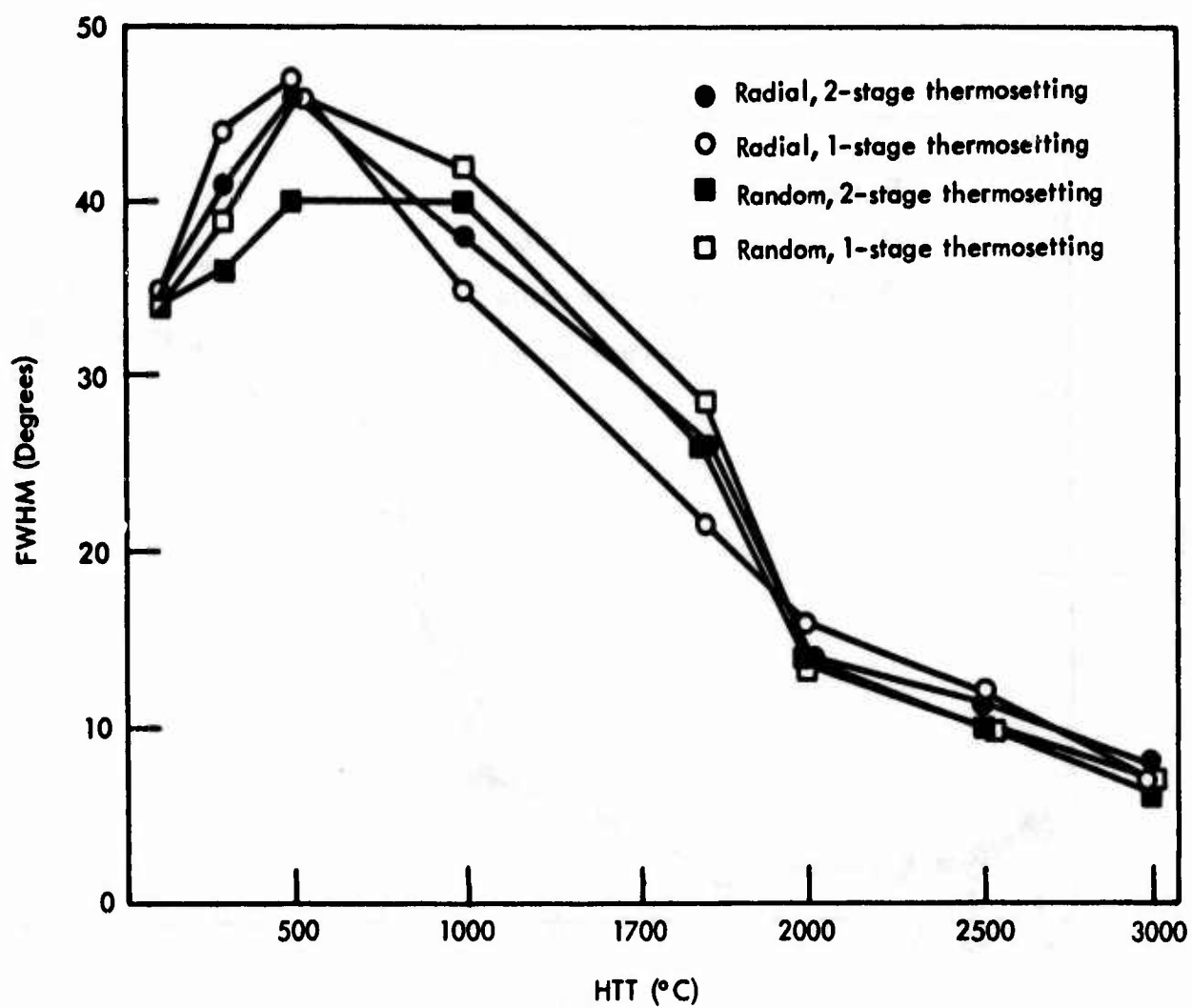
G760194

Figure 12.   Preferred orientation (FWHM) as a function of HTT
for Type P fibers with radial and random structures,
thermoset by two different methods.
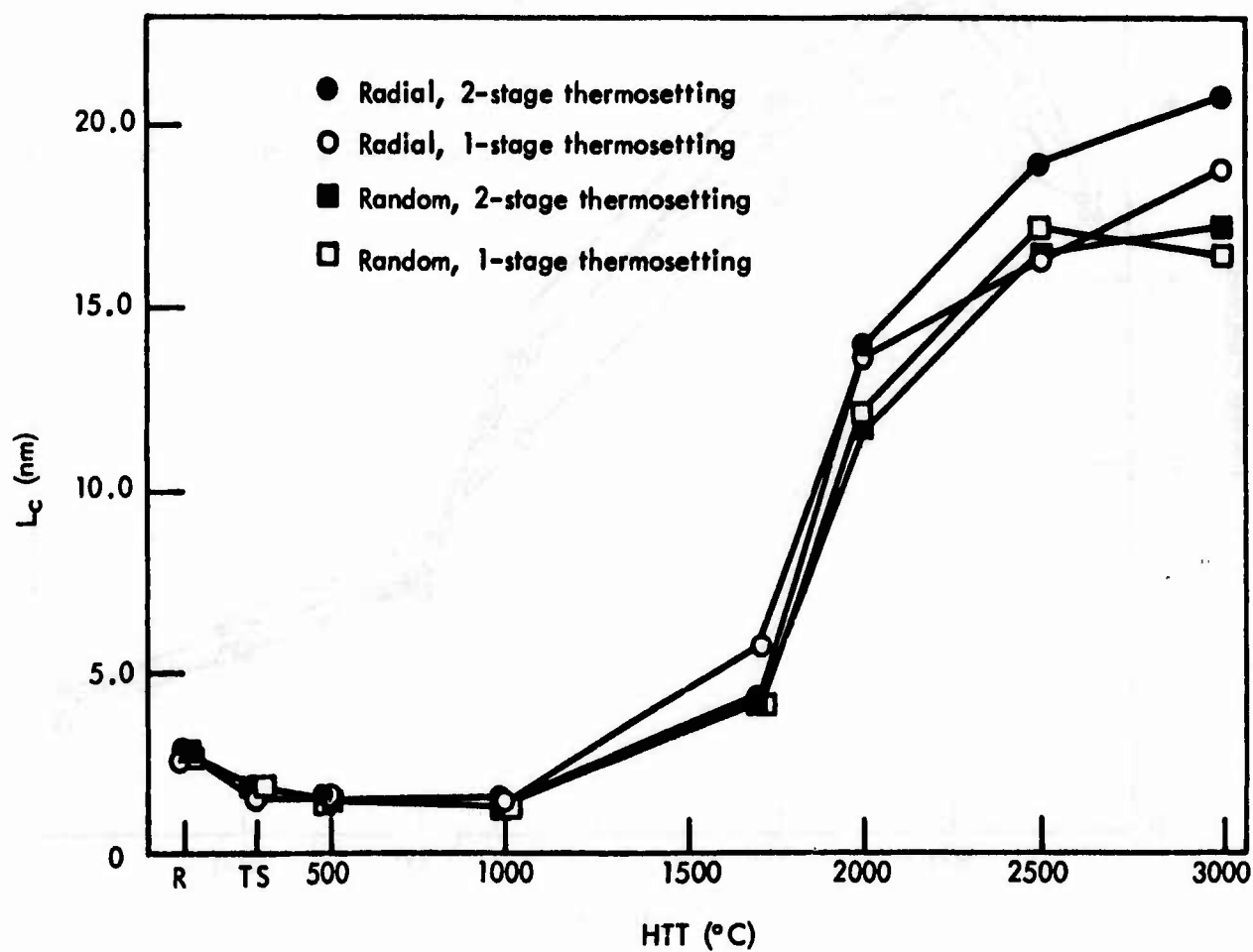
35

Figure 13. The development of crystallite size (L_c) as a function of HTT of fibers with different structures, thermoset by two different methods.
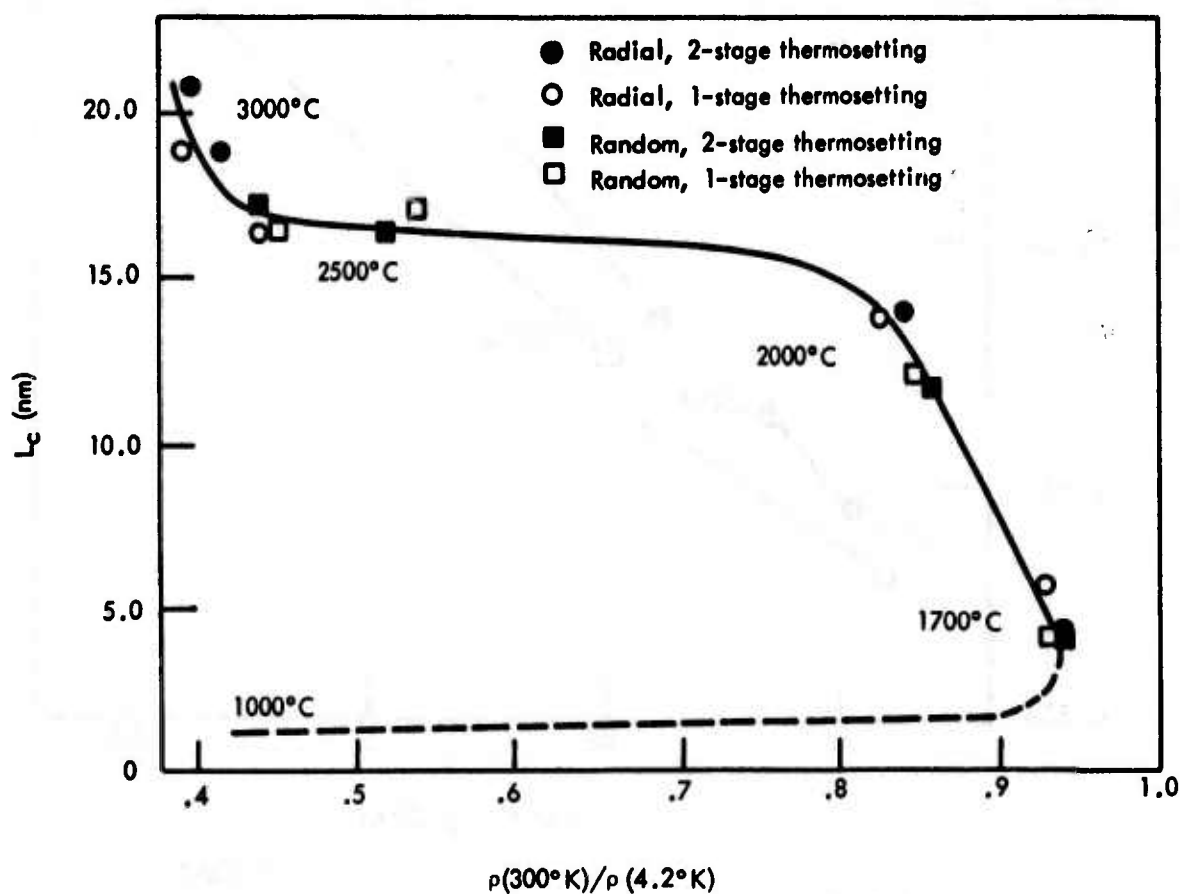
Figure 14.   Crystallite size L_c as a function of
resistivity ratio for fibers with different
structures. (The temperatures indicate
the levels of HTT).
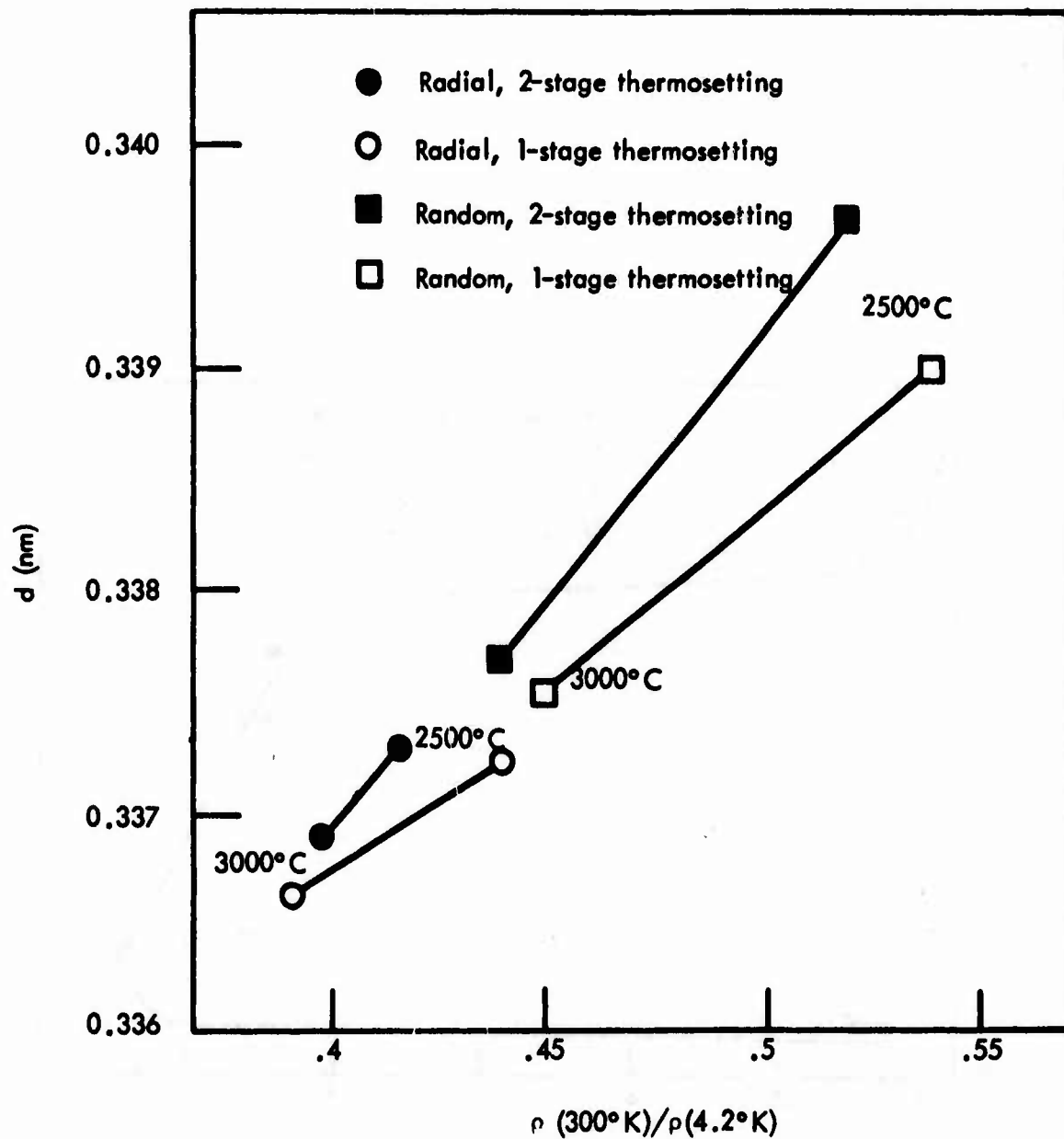
Figure 15. d-spacing of the graphite lattice as a function of the resistivity ratio. (The temperatures indicate the level of HTT.)

38

4. Mechanical Properties

The Young's modulus, tensile strength and density of the yarn filaments are summarized in Table XII. For comparison, the X-ray preferred orientation and the resistivity ratio are also indicated. In all four series of fibers, the modulus increases steadily with HTT to a value near 700 GPa (100 Mpsi) at 3000°C. This occurs simultaneously with a steady increase in density and a decrease in the FWHM and the resistivity ratio (except from 1000°C to 1700°C). The tensile strength, on the other hand, shows a more complicated dependence on HTT, as shown in Figure 16. The tensile strength of these random structure fibers is higher at low HTT than that of these radial structure fibers. Above 2500°C HTT, however, the tensile strength of the random fibers does not increase while the strength of the radial fibers continues to increase sharply and eventually exceeds that of the random fibers. Presumably, this results from the different degree of graphitizability of the two structures. Fibers thermoset by the two-stage process tend to be stronger than those with the same structure thermoset by the one-stage process. In all cases, the strength decreases as HTT increases from 1700°C to 2000°C, and then increases again at higher HTT. The reason for the decrease is not clear. A possible explanation is based on the fact that the fibers treated at 2000°C and higher were heated in a furnace that may have been contaminated. Traces of silicon or other impurities diffusing into the fibers could adversely affect the tensile strength.

The modulus correlates generally with resistivity ratio, as would be expected because both evolve in more or less predictable ways as HTT is increased. The large experimental uncertainties in the modulus values make it impossible to say whether there is a detailed correlation, i.e., for different structure fibers at the same HTT. Note that the resistivity ratio depends on the degree of graphitization while the modulus depends mostly on preferred orientation. Thus, there is no particular reason to expect a detailed correlation in this case. The relationship between modulus and preferred orientation is shown explicitly in Figure 17. The correlation appears to be quite good, in spite of the large uncertainties in modulus values.

An attempt was made to relate the magnetoresistance of the fibers to the modulus and the orientation. It was found, however, that the MR behaves sufficiently differently for different degrees of graphitization that no simple correlation can be drawn between magnetoresistance and modulus. Even at a given HTT, the variability of the graphitizability of different filaments prevents a direct correlation from being made. It is certainly true, nonetheless, that the magnetoresistance does depend on preferred orientation; it may be possible to deconvolute it to obtain a measurement of preferred orientation if a suitable model of the electronic structure can be found.

5. Conclusions

This study has shown that reproducible correlations exist between various electrical, mechanical and structural properties of Type P fibers. The resistivity at room temperature, the resistivity ratio and the transverse magnetoresistance are well correlated with each other; knowledge of one of these parameters (e.g., the resistivity ratio, which is easiest to measure) allows one to predict the values of the others with reasonable accuracy.

39

TABLE XII

Mechanical Properties of Type P Fibers with Different Structures and Thermosetting

Material	HTT	Modulus, GPa	Tensile Strength, GPa	Density	FWHM, Degrees	R (300)/ R (4.2)
Radial -	1000	85.2	0.956	1.72	38°	-
Two Stage	1700	209	1.48	2.07	26°	.938
	2000	358	1.38	2.17	14°	.842
	2500	610	1.32	2.20	11.5°	.417
	3000	679	2.30	2.21	8°	.398
Radial -	1000	90.4	0.709	1.74	35°	-
One Stage	1700	207	1.21	2.10	21.5°	.929
	2000	338	1.08	2.17	16°	.826
	2500	692	1.80	2.18	12°	.441
	3000	708	2.78	2.19	7°	.392
Random -	1000	91.2	0.996	1.68	40°	.435
Two Stage	1700	182	2.01	1.98	26°	.94
	2000	383	1.51	2.09	14°	.86
	2500	540	2.01	2.16	10°	.52
	3000	698	2.03	2.18	6.2°	.44
Random -	1000	85.4	0.866	1.69	42°	-
One Stage	1700	170	1.38	1.99	28.5°	.926
	2000	336	1.28	2.11	13.7°	.848
	2500	587	1.72	2.15	10°	.54
	3000	657	1.83	2.17	7°	.45
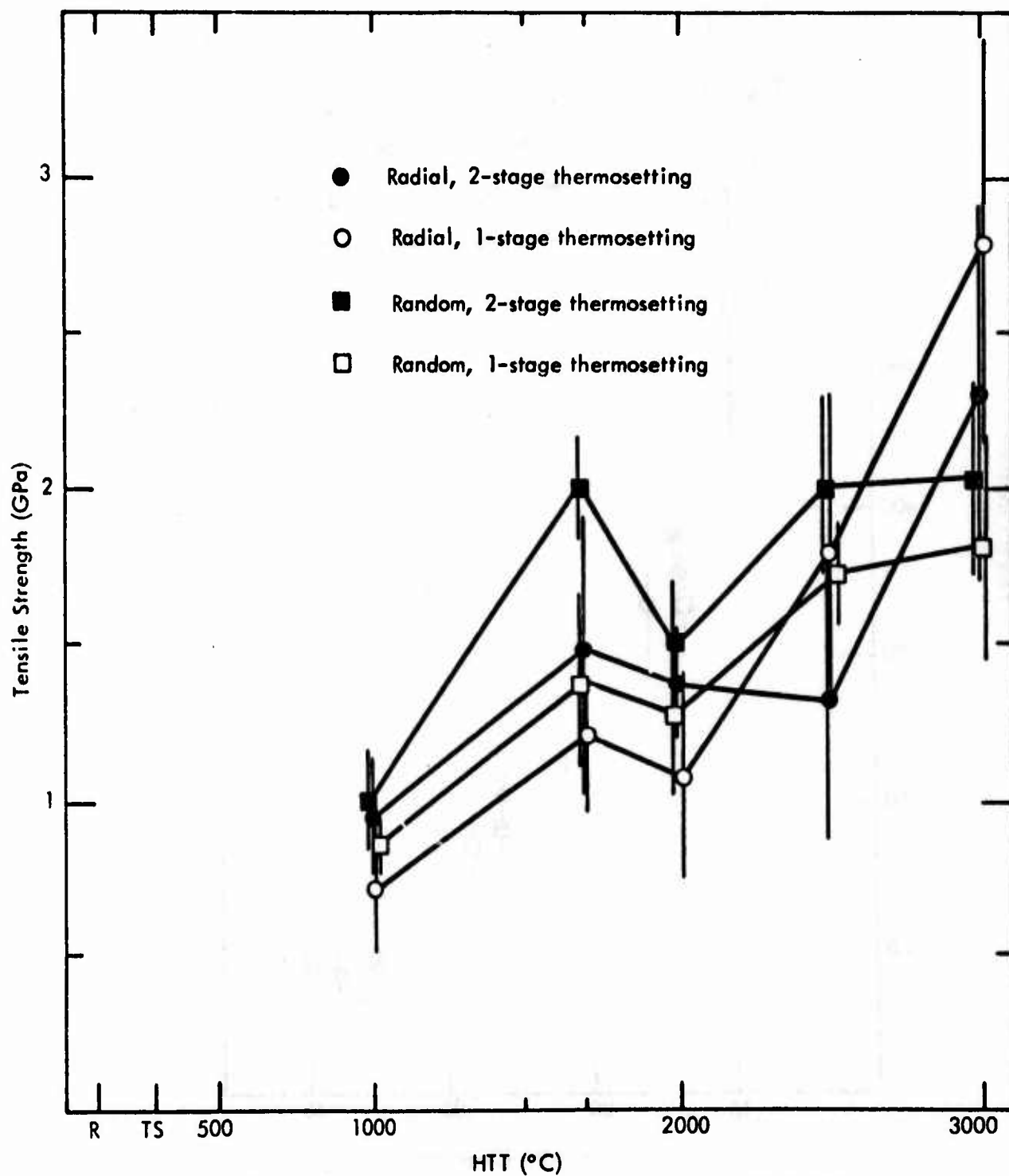
Figure 16.   Tensile strength of fibers with radial and
random structures as a function of HTT.

41
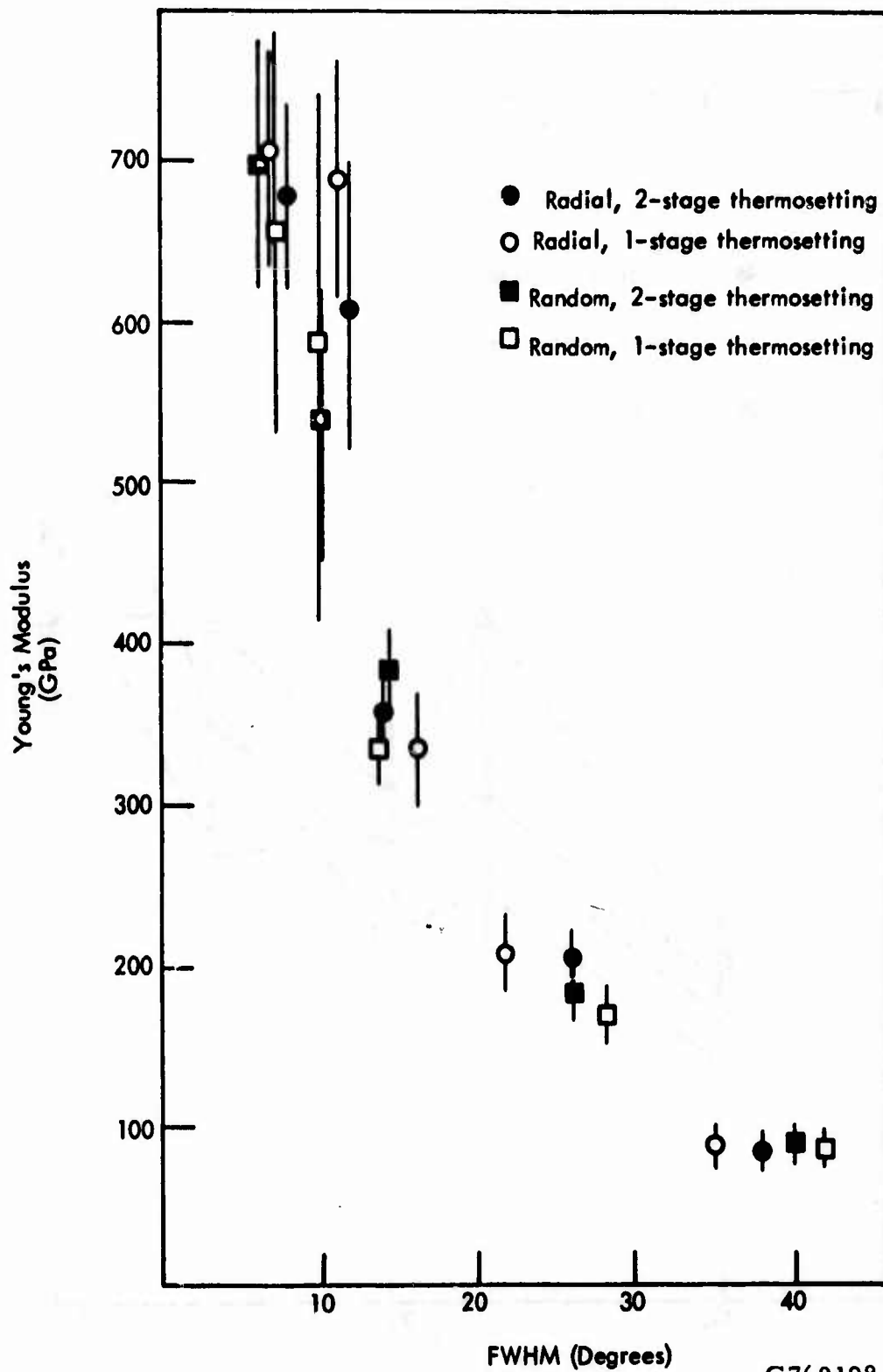
Figure 17. Young's modulus as a function of orientation (FWHM) for fibers with random and radial structures, thermoset by two different methods.

These electrical properties are also related to several structural parameters of the fibers: the interlayer spacing (d), the stack height (L_c), and the degree of 3-dimensional order. All six of the above named parameters depend primarily on (or, in some cases, determine) the degree of graphitization of the sample. The close correlations between these parameters are, then, not surprising.

Predictably, the Young's modulus correlates well with preferred orientation in the fibers. There is also a correlation between modulus and degree of graphitization, but it is not clear whether this is direct or indirect (via a correlation between preferred orientation and graphitization). Tensile strength does not correlate well with any other electrical or structural parameter. None of the parameters studied here correlates more than approximately with heat-treatment temperature. This implies that HTT is not a good indicator of degree of graphitization, i.e., that other factors such as details of the structure, also have an important influence on the graphitization process. Strong supporting evidence was found in this study. At heat-treatment temperatures above 1700°C, significant differences in the degree of graphitic character were observed between fibers with radial and random structure. The radial fibers were more graphitic at a given HTT and reached a higher ultimate degree of graphitization at the highest HTT than the random fibers subjected to an identical treatment. The most likely explanation for this is that the random structure is more highly defected and grain growth is inhibited at an earlier stage than in the radial structure.

Differences in the thermosetting procedure were found not to have any systematic effect on the electrical or structural properties of the fibers after heat treatment. The two-stage process resulted in higher tensile strengths than the one-stage process. It is not clear at this writing why this is so.

Finally, it is useful to compare the mesophase pitch-based fibers with other carbon systems. The electrical measurements suggest that these fibers are very similar to pyrolytic carbons treated in the same temperature range. This is consistent with the high degree of graphitization attainable in Type P fibers. On the other hand, PAN-based fibers have been found to exhibit a much lower degree of 3-dimensional order than Type P fibers subjected to an identical high temperature treatment.

SECTION V

STRUCTURE OF FILAMENTS IN TYPE P YARN

The various microscopic methods used to study the structure of pitch and carbon filaments have been described in a previous Technical Report.[8] Three broad classifications for transverse structures in the as-spun and carbonized fibers (radial, onionskin and random) have been identified by polarized light microscopy. Carbonized radial fibers usually have a "missing wedge," but random and onionskin fibers are cylindrical. The results of continued structural studies by optical microscopy and SEM will be discussed in this section.

1. Fiber Structure Terminology

During the current contract period, most of the structural studies have dealt with multifilament yarn samples containing significant numbers of cracked ("missing wedge") and round fibers. In the course of these studies, it has become apparent that classifying a given fiber structure as either radial, random, or onionskin is an oversimplification. Fiber structures ranging more or less continuously from pronounced radial to pronounced onionskin have been observed. Carbonized fibers having a crack angle of 90° - 180° almost always have a pronounced radial structure, but the situation is more complex for crack angles less than 90°. As a first approximation, the crack angle can be used as a measure of the degree of "radial character" (with the larger crack angles corresponding to a more radial structure) in a given sample, but this criterion may not be sufficient when comparing filaments having the same crack angle in different yarn samples. Furthermore, fibers that do not have a crack can vary from random to a weakly radial structure in multifilament yarn, depending on the sample examined. Round monofilament fibers have structures ranging from onionskin to random. Since the situation is so complex, it would be cumbersome to attempt a description of the fiber structures in terms of both their crack angle and degree of radial character, particularly without a quantitative measure for the latter. For that reason, the description of fiber structure in this section will be limited to the terms cracked and round.

2. Correlation of Fiber Structure with Single Filament Properties

The first effort to correlate fiber structure with single filament properties for a multifilament yarn sample was described in the final report for the previous contract period.[9] The results are summarized in Table XIII for yarn sample LTF-17E. The single filament properties were identical within experimental error for the fibers classified as round and cracked. The cracked fibers had a somewhat greater cross-sectional area than the round fibers. Unexpectedly, five out of twenty-four fibers in this sample were found to change from a cracked to a round structure within a length of ~ 3 cm. The filaments with such variable structure had somewhat lower tensile strength and Young's modulus than the cracked or round fibers.

TABLE XIII

Summary of Filament Properties for Sample LTF - 17E

	Fiber Area (μ m²)		Young's Modulus (GPa)		Tensile Strength (GPa)	
	Fiber Test	Optical Microscopy	Fiber Test	Optical Microscopy	Fiber Test	Optical Microscopy
Both Ends Round (n=14)	33.9 ± 6.7	38.3 ± 7.8	270 ± 90	240 ± 75	2.2 ± 0.3	2.0 ± 0.2
Both Ends Split (n=5)	39.2 ± 5.2	50.9 ± 4.4	360 ± 190	270 ± 105	2.3 ± 0.3	1.8 ± 0.2
One End Round One End Cracked (n=5)	36.0 ± 4.6	45.9 ± 5.0	235 ± 34	183 ± 19	1.6 ± 0.8	1.2 ± 0.5
All Fibers With Both Ends (n=24)	35.1 ± 6.1	42.6 ± 9.4	284 ± 112	235 ± 80	2.1 ± 0.5	1.8 ± 0.4

To confirm these findings, a second multifilament yarn sample containing round and cracked fibers was investigated using an almost identical procedure. Single filament tests (19.8 mm gauge length) were obtained for 40 filaments. Both ends of the mounting tab for each filament were preserved and optical micrographs of the portion of the filament remaining on each end of the tab were obtained. The micrographs were used to classify each filament according to structure (round or cracked) and to measure the cross-sectional area of the filaments with a planimeter. The average of the two area determinations for each filament was used to recalculate Young's modulus and tensile strength for each filament.

The properties of the round and cracked filaments in this yarn sample are shown in Table XIV. Optical micrographs of both ends of the filament were obtained for 31 of the 40 fibers tested. Nineteen were cracked on both ends, six were round on both ends, and six were cracked on one end and round on the other end. The structural variation along the length of some filaments was expected because the microscopic observations, that will be described in the next subsection, had shown that about one fourth of the fibers in this yarn sample could be expected to undergo structural changes over a length of ~ 3 cm.

The data in Table XIV show that the fiber cross-sectional area obtained from the optical micrographs for all fibers was significantly greater than the area determined in our standard single filament testing. This result differs from that obtained for sample LTF-17E and is contrary to expectations. The largest difference between the two area measurements would be expected for cracked fibers because the single filament testing method (split-image microscope) measures the minimum shadow diameter, which should lead to an erroneously small cross-sectional area of cracked fibers. Since this behavior was not found, it appears that variations in the area in all fibers, regardless of structure, are greater than the expected error in measurements for cracked fibers. The optical microscopy measurements of filament cross sections produces results closer to the average cross-sectional area because the two points on the fibers that are measured are selected more or less randomly. An average cross-sectional area variation of 15% was estimated by comparing the optical micrographs of the two ends of the same filament. It is known from polymer spinning that such fluctuation of diameters along the fiber can occur as a result of draw resonance.[10]

The cross-sectional areas of round, cracked and "mixed" filaments were the same in the sample 280-23-39I. The values calculated from the optical microscopy area measurements for Young's moduli and tensile strengths of the round, cracked and "mixed" fibers are the same within the experimental error, confirming the results of the study on sample LTF-17E. Although the results are somewhat clouded by the structural variations along the length in the filaments and the relatively large standard deviations, the difference in the Young's moduli between round and cracked fibers is unlikely to be more than about 25%. Davis and Sullivan[11] had reported that the Young's modulus of the cracked filaments was about 50% greater than that of the round ones in the samples they investigated. Considering the differences in the yarns used, it is probably not worthwhile to speculate on the reasons for the discrepancy.

TABLE XIV

Summary of Filament Properties for Sample 280-23-391

	Fiber Area (μm^2)		Young's Modulus (GPa)		Tensile Strength (GPa)	
	$FT^{(1)}$	$OM^{(2)}$	$FT^{(1)}$	$OM^{(2)}$	$FT^{(1)}$	$OM^{(2)}$
Both Ends Round (n=6)	36 ± 10	57 ± 14	300 ± 40	190 ± 20	1.9 ± 0.3	1.2 ± 0.2
Both Ends Split (n=19)	47 ± 7	58 ± 7	250 ± 30	200 ± 40	1.2 ± 0.3	1.0 ± 0.3
One End Round One End Cracked (n=6)	46 ± 10	62 ± 12	260 ± 30	190 ± 10	1.6 ± 0.3	1.2 ± 0.2
All Fibers With Both Ends (n=31)	45 ± 9	59 ± 9	260 ± 40	200 ± 30	1.4 ± 0.4	1.1 ± 0.3

(1) Averages and standard deviations for filament properties and cross-sectional area from long gauge (19.8 mm) filament testing (FT).

(2) Averages and standard deviations using areas measured on optical micrographs (OM) to recalculate filament properties.

47

The Young's moduli and tensile strengths are lowered from 260 to 200 GPa and from 1.4 to 1.1 GPa, respectively, when the fiber areas determined from the optical micrographs are used for calculations. Previous single filament tests on this yarn sample showed a Young's modulus of 260 GPa and a tensile strength of 1.5 GPa, while the strand test showed a modulus of 190 GPa and a tensile strength of 1.2 GPa. The strand test results agree closely with the single filament test results calculated from the areas determined from the optical micrographs because both methods use the average fiber area to calculate the properties, while the minimum filament area was used in the conventional single filament tests in the past. It is arguable whether filament or strand properties give a more accurate measurement of filament properties, but strand properties are generally more useful in predicting the behavior in composites. For that reason, the single filament testing method was modified to compute the cross-sectional area from several diameter measurements taken along the filament. This modification was used in the single filament testing described in other sections of this report. It resulted in decreasing the average properties of single filaments, but large discrepancies between single filament and yarn tests still exist. Their origin must be sought in factors other than the measurement of the filament diameter. (See Section VI).

3. Optical Microscopy of Filaments with Variable Structure

The structural variations along some Type P yarn filaments, described in the previous section, were substantiated by additional microscopic studies. Eight individual filaments from samples LTF-17E and 280-23-39I were sectioned at ~ 10 mm intervals and micrographs of the fiber cross section at these intervals were examined. The structure of two of the filaments in each sample changed from round to cracked over a 50 - 100 mm length. The other six fibers in each sample did not change in structure over this length. These results confirmed the evidence in Tables XIII and XIV that about one-fourth of the filaments in yarn samples LTF-17E and 280-23-39I change from a round to cracked structure within a length of several centimeters. Since the reasons for this behavior were not apparent, a more detailed optical microscopy investigation of the structural variation along the length of the filaments was initiated.

The approach that was used involved sectioning a single filament into ~ 1 cm lengths, encapsulating all of these sections in a single metallographic specimen mount, and then polishing down the specimen mount at ~ 1 mm intervals. Whenever examinations of a polished section revealed that the structure of the filament was changing significantly, then the sectioning interval was reduced so that the structural variation near the point where the crack disappeared could be followed on an even finer scale. In addition to the structural observation, filament cross-sectional area measurements at each interval were made to obtain more data on the variation of this parameter.

The specimens used for this work were the four mounts containing the ~ 1 cm sections of the variable structure filaments from samples LTF-17E and 280-23-39I. In general, the periodic disappearance and appearance of the crack in these samples was confirmed beyond doubt. In two of the filaments, the region near the crack termination point was located. No foreign particles

or obvious carbonaceous inclusions were found in these regions. The internal fiber structure, revealed in polarized light, gradually changed from cracked, moderately radial to round, less radial or random. In two filaments, micrographs of some 1 mm sections revealed what appeared to be an inclusion or a pore, but these were not close to a crack termination point. Furthermore, the crack seemed to follow a spiral path along the length of all four filaments. This behavior is shown in Figure 18; the filament length between micrographs 2A and 3A is ~ 1 cm and the length between 2A and 2B or 3A and 3B is ~ 1 mm. The micrographs show that there is a significant crack rotation in a length of ~ 1 mm. This degree of crack rotation is much greater than could be expected from any twist put into the filament during specimen mounting. Cross-sectional area measurements were made with a planimeter on all the micrographs obtained during the ~ 1 mm section study. These measurements showed that the cross-sectional area of the cracked portion was the same as that of the round portion for each of the filaments. In fact, the data summarized in Table XV show that the cross-sectional area of these four variable structure filaments was quite uniform.

The detailed optical microscopy study of these four filaments was very time consuming. Therefore, it was terminated after polishing down about 4 mm at intervals of ~ 1 mm. Further studies of the nature of the crack and its rotation were conducted by SEM as will be described in the next subsection.

An optical microscopy study was also performed on a third multifilament yarn sample (571-20-24A) that contained significant amounts of cracked and round filaments. Optical micrographs of this yarn sample are shown in Figure 19. They are similar to micrographs of yarn samples LTF-17E and 280-23-39I. Twenty single filaments from 571-20-24A were selected and sectioned into 1 cm lengths and all of the sections for each filament were encapsulated in one or two metallographic specimen mounts. Optical micrographs were obtained for each section and the cross-sectional area of the section in each micrograph was measured with a planimeter. The number of micrographs for a single filament varied between 4 and 10. Six filaments were cracked, seven filaments were round, and seven filaments changed from cracked to round in the length examined. The area measurements are summarized in Table XVI. The cross-sectional area uniformity of the individual filaments in all three structural classifications was the same within experimental error. Thus, the cracked sections of the variable structure filaments have the same cross-sectional area as the round sections. There is considerable filament-to-filament variation in cross-sectional area in each structural classification, but the average area for the cracked, round and variable filaments is the same, even though the cracked fibers appear to be larger than the round fibers in the micrograph of the yarn cross section (Figure 19). The cracked fibers had a larger area than the round fibers in only one sample (LTF-17E) of the three studied. Only one filament in sample 571-20-24A showed a large variation in the cross-sectional area along its length. This filament, shown in Figure 20, had a variable structure. One of the ten sections for this filament had a much larger area than the others and this section also appeared to contain an inclusion. An attempt was made to determine the elemental analysis of the inclusion in the scanning electron microprobe, but accurate data could not be obtained because the inclusion was too small.
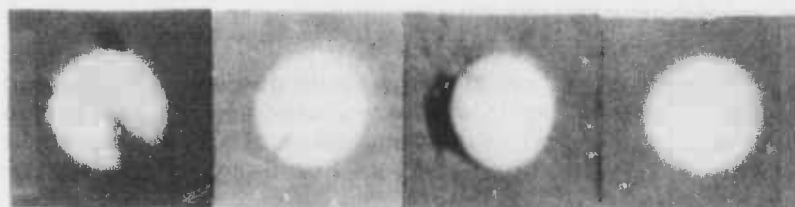
49

2A   2B   2C   2D

3A   3B   3C   3D

Figure 18. Optical micrographs of ∼ 1 mm sections of a variable structure filament from Sample LTF-17E. Cross-sections 2A - 2D and 3A - 3D are from the first and the third 1 cm sections, respectively, of the same filament. Magnification, 2000X.
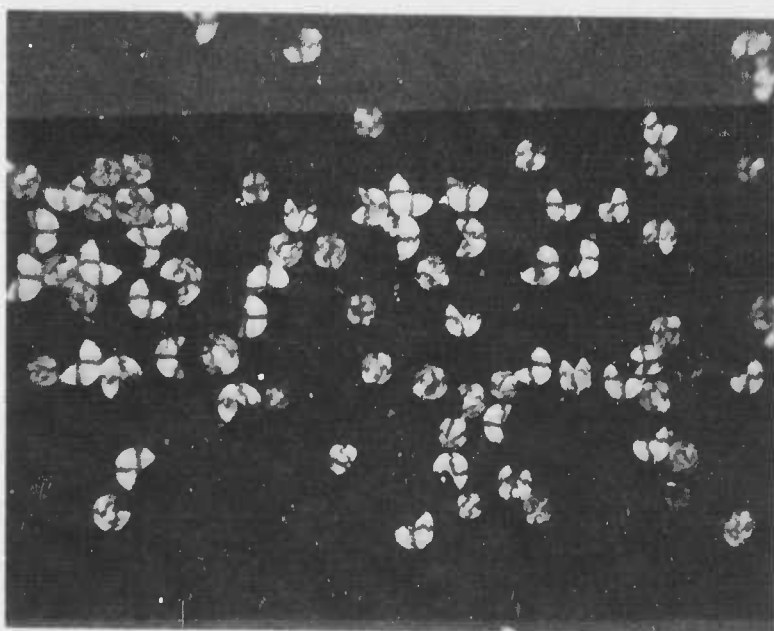
TABLE XV

Cross-Sectional Area Measurements of Variable

Structure Filaments in Samples LTF-17E and 280-23-39I

Filament	Filament Length (cm)	Number of Measurements	Average Cross-sectional Area (μm^2)
280-23-39I-3	5	28	50.2 ± 4.2[1]
280-23-39I-4	4	36	67.0 ± 2.2
LTF-17E-E	8	66	50.0 ± 2.9
LTF-17E-G	8	84	47.2 ± 2.4

[1] Standard Deviation

51
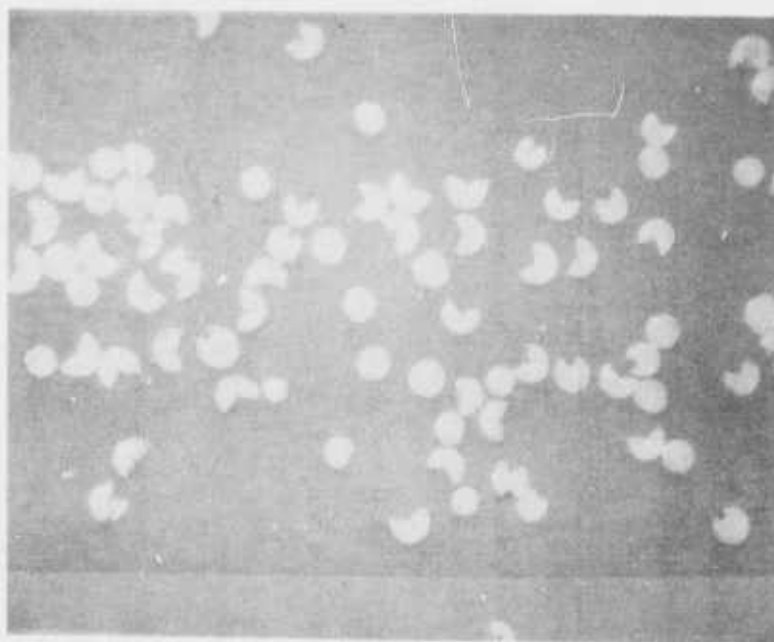
(a) 500X

(b) 500X

Figure 19. Optical micrographs of yarn sample 571-20-24A in bright
field (a), and in polarized light (b).

TABLE XVI

Summary of Cross-Sectional Areas Measurements of Filaments in Sample 571-20-24A

Structure	Filament Number	Average Cross-Sectional Area (μm^2)	Average Area* Deviation (μm^2)
Cracked	1	78.2	2.8
	2	84.5	4.2
	3	45.9	1.0
	5	98.4	5.7
	8	42.5	3.5
	16	85.8	2.1
		Average = 72.6	Average = 3.2
Round	4	42.7	1.1
	6	40.3	2.4
	11	107.2	2.5
	15	84.1	4.8
	17	79.7	2.4
	18	82.0	0.9
	19	75.9	1.5
		Average = 73.1	Average = 2.2
Variable	7	62.8	3.6
	9	56.8	5.0
	10	69.1	3.8
	12	74.1	2.8
	13	57.4	1.4
	14	67.7	0.6
	20	78.8	1.6
		Average = 66.7	Average = 2.7

* Average area deviation = Σ 1An - $\overline{A}$l/n, where An is the area for a given section, $\overline{A}$ is the average cross-sectional area for the filaments and n is the number of areas measured for that filament.

53

2 3 4 5 6
(53) (59) (53) (55) (51)
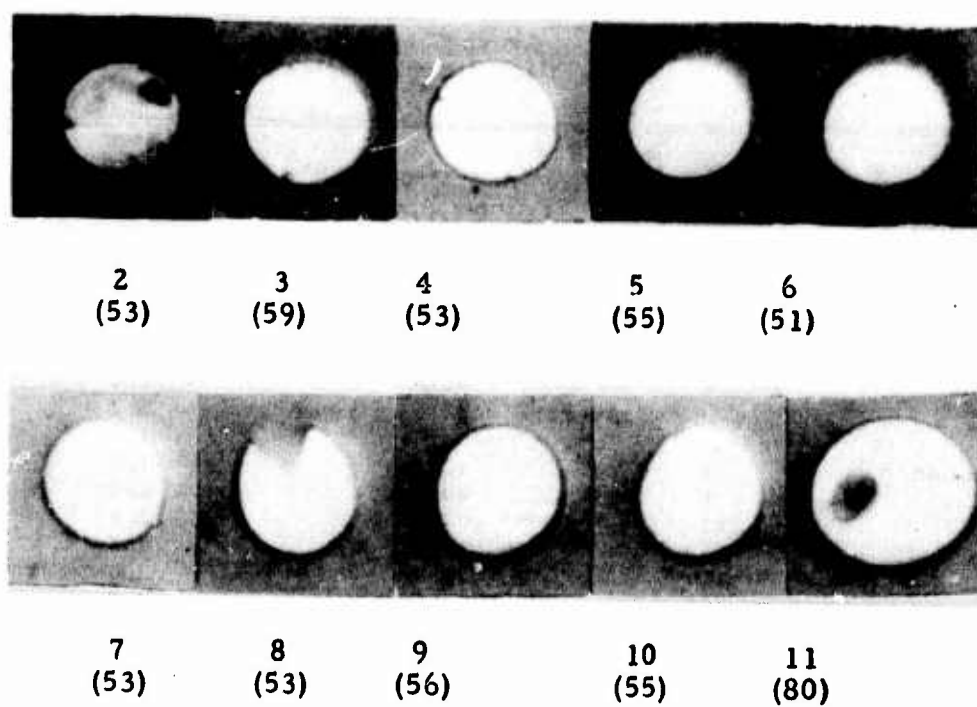
7 8 9 10 11
(53) (53) (56) (55) (80)

Figure 20. Optical micrograph of consecutive sections (1 mm apart) of filament No. 9 in Table XVI. Cross sectional area in μm^2 listed below section number. Magnification, 2000K.

In some yarn samples, cracks were observed which did not propagate all the way to the center of the filaments. Figure 21 represents schematically a partial view of one such yarn through a quarter-wave plate under the polarized light microscope.[12] The color distribution in the partially cracked filaments clearly proves that these filaments have a radially oriented outer rim and a core with an onionskin structure. The crack does not propagate through this inner core.

4. SEM Studies of Yarn Samples with Mixed Filament Structures

SEM examinations were made on yarn samples 280-23-39I and 571-20-24A to obtain more information regarding the nature of cracks and crack spiraling. The results were very illuminating. While most of the filaments in which a crack was visible remained cracked for a length of ~ 2 cm, a significant number of filaments were found where the crack termination point was visible. Figure 22 shows two such filaments from sample 280-23-39I. No inclusions were detected at any of the crack termination points in either sample. In some cases, such as that shown for the lower fiber in Figure 22, both ends of a given crack were found. The crack is only 0.5 mm long and the crack spiraling is apparent. Many other cracked filaments exhibited similar spiral cracks which often changed their direction of rotation within a length of 2 cm. Moreover, the crack angle varied from ~ 45° to less than 10° during the crack spiraling in one filament. The angle of crack rotation seemed to vary from barely perceptible in the SEM to more than 90° in a length of 0.5 mm, depending on the filament examined. Another example of crack termination and spiraling is shown in Figure 23 for yarn sample 571-20-24A. Similar results have been recently reported by other investigators.[13]

In many filaments of both samples, two crack termination points were found in the same region. The middle photograph in Figure 23 and the two examples shown in Figure 24 are typical of this feature. These regions are probably weak points in these filaments. It appears that the stresses in the fiber near these "double crack" points had been quite high during processing; consequently, both fibers in Figure 23 seem to have delaminated near the crack termination points. An extreme example of the double crack is shown in Figure 25. This filament has five double crack regions within a length of ~ 0.5 mm. Fortunately, such features are not typical of Type P carbon fibers. The more common behavior is shown in Figure 25 by the filament above the multicracked fiber; the crack is straight and does not change its angle for a length of 0.5 mm. All findings with the scanning electron microscope are completely consistent with the detailed results of optical microscopy described previously. Moreover, the SEM observations greatly aided in interpreting some of the optical data.

The crack lengths determined in the SEM range from ~ 0.5 mm to the entire length of ~ 2 cm visible in the SEM. The finding of such extremely short crack lengths is disturbing because it casts some doubt on the validity of the structural classification method used in the investigation of fiber properties vs. structure described in Section V-2. In that investigation, a fiber was classified as cracked if two optical cross sections, separated by a length of ~ 4 cm, were cracked.
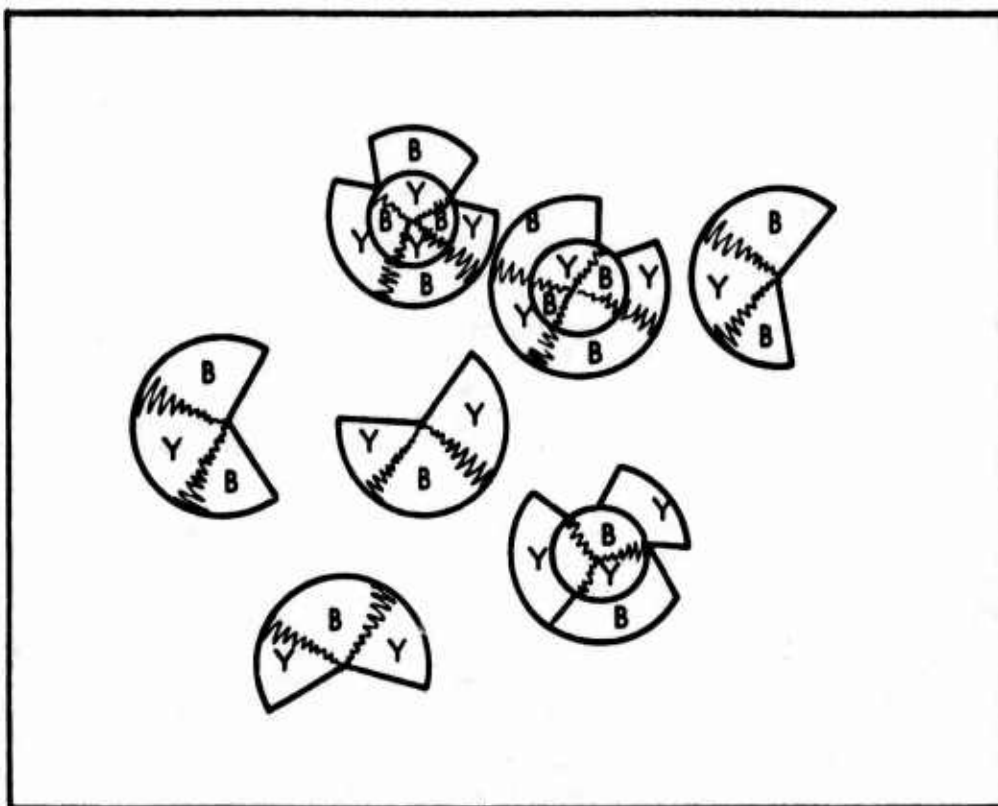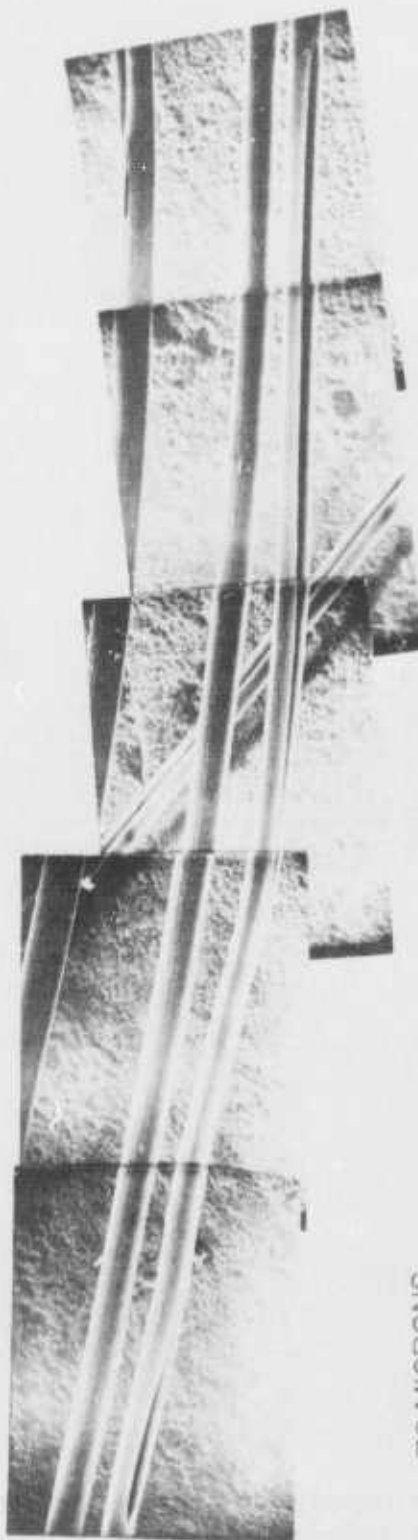
G760203

Figure 21. Sensitive tint view of cracked filaments showing
mixed radial/tree-trunk structures. (Schematic
representation, Y = yellow, B = blue).

3 MICRONS

70 MICRONS

Figure 22. Composite photomicrograph of filaments in yarn sample 280-23-39I observed in SEM.
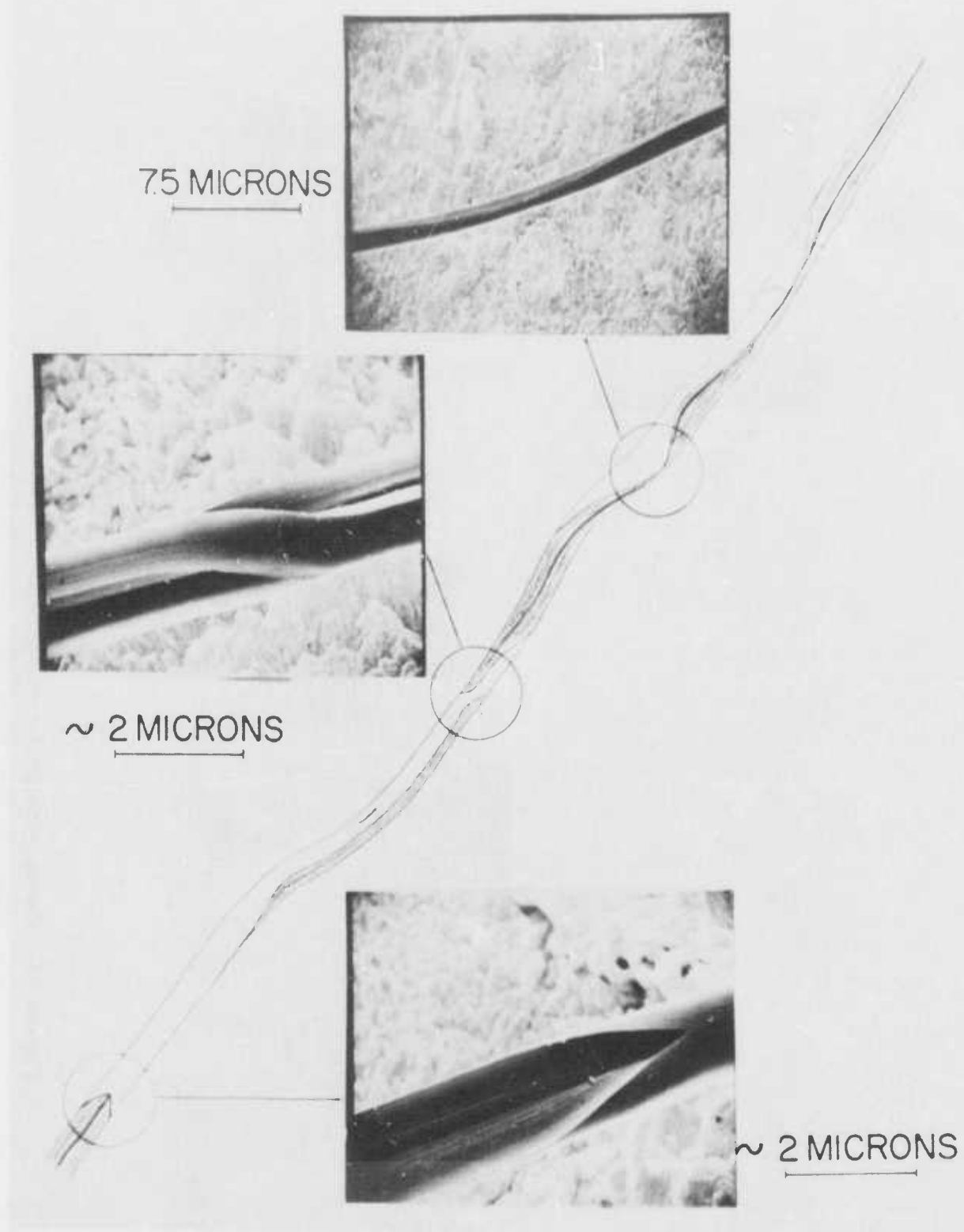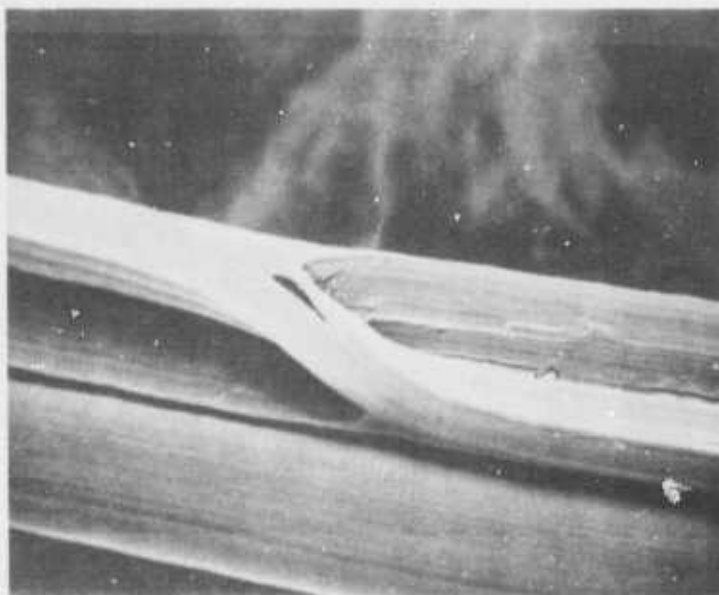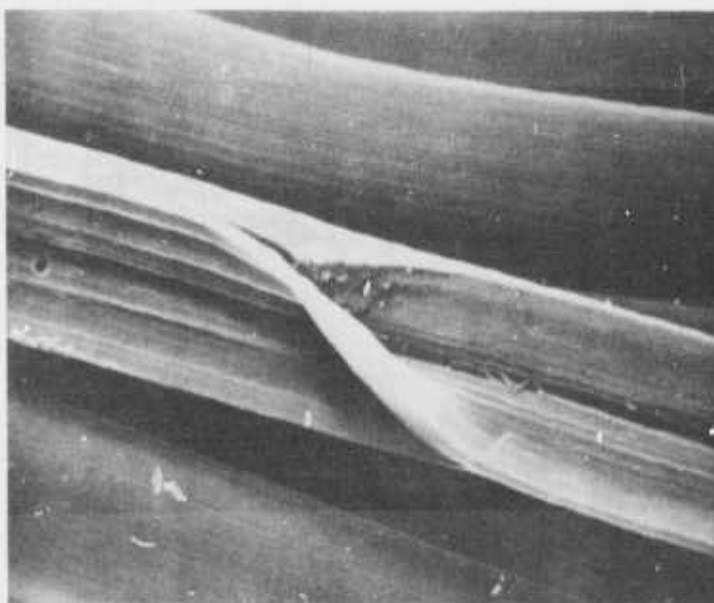
7.5 MICRONS

~ 2 MICRONS

~ 2 MICRONS

Figure 23. Schematic diagram and SEM views of a filament in Sample 571-20-24A. Fiber diameter exaggerated in drawing for clarity.

(a) 1500X

(b) 1500X

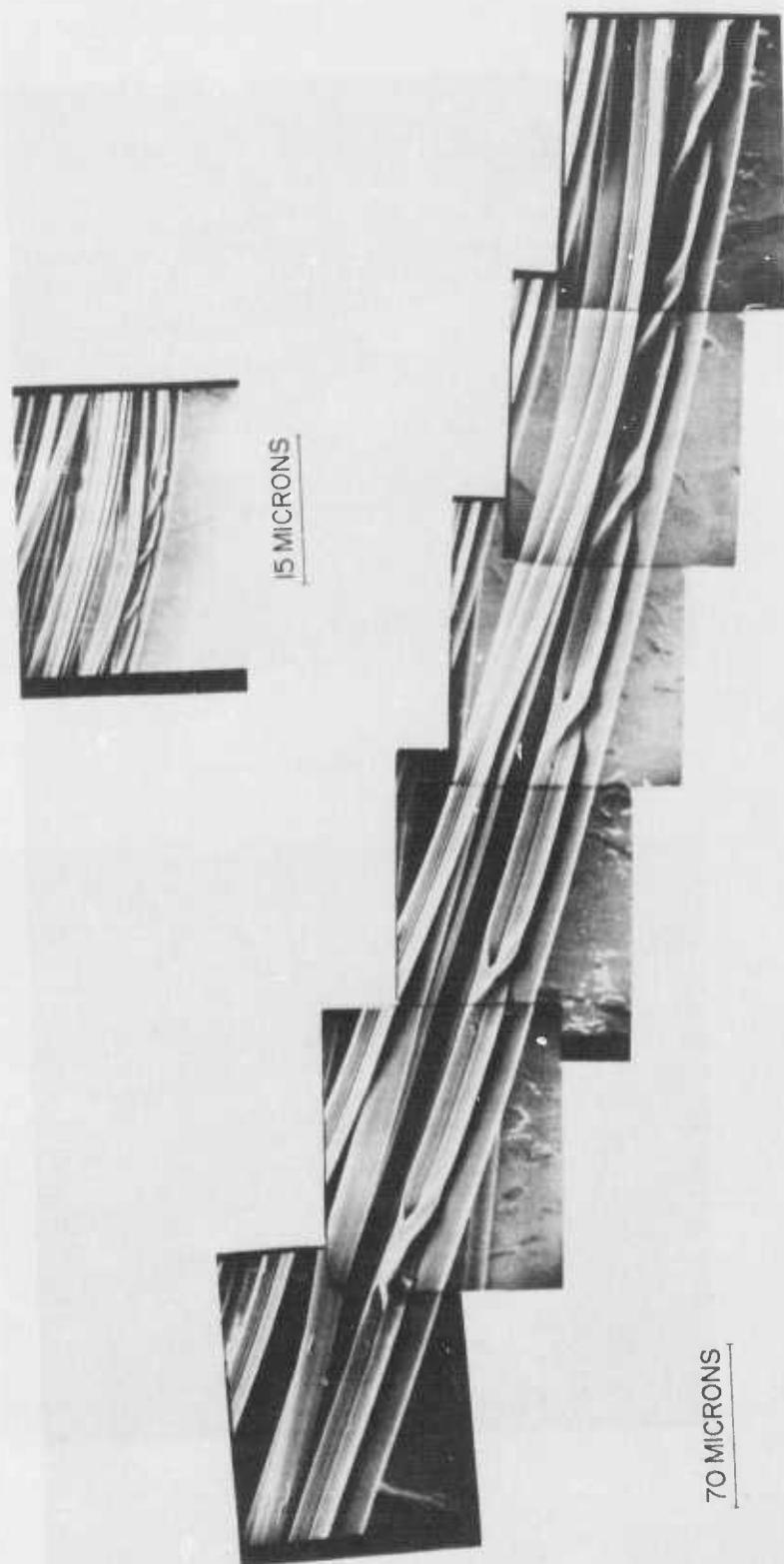Figure 24. SEM views of filaments in yarn sample 571-20-24A.

15 MICRONS

70 MICRONS

Figure 25. Composite photomicrograph of filaments in yarn sample 571-20-24A, observed in SEM.

60

The SEM results indicate that the filament structure could change several times in this length. Similar considerations apply to the filaments classified as being all round.. Potential errors in the classification could explain why the properties of the filaments classified as round were the same as those classified as cracked.

It also should be noted that the structural information described above has been obtained on only three yarn samples of the type where both round and cracked fibers are present in significant amounts. This type of yarn sample was selected for study because it was believed that it would be possible to determine the differences between the properties of round and cracked filaments without the potential complexities of lot-to-lot differences in pitch precursors and processing conditions that were expected if yarn samples containing either predominantly cracked or predominantly round fibers had been selected. It is now clear that the cracked fibers in the mixed yarn samples can differ in crack angle, degree of radial character, etc. Herein, perhaps lies the reason why it is not possible to establish clear correlations between fiber structure and properties at this writing. It is also clear, however, that the presence of short, twisted cracks, and particularly of crack ends meeting each other, must result in an accumulation of undesirable stresses to the detriment of filament strength. Consequently, it is not surprising that highest tensile strengths have been measured throughout this entire study on fibers which are completely free of such cracks.

5. SEM Examination of Mating Fracture Surfaces

Almost all fracture surfaces for SEM examination were generated by manually breaking fiber bundles of yarn in air. It is possible that some of the surfaces produced by this procedure may not have been the original fracture surfaces because the brittle nature of high modulus carbon fibers often leads to a secondary fracture from the "springback" which follows the initial fracture. True fracture surfaces for SEM examination were prepared by breaking individual filaments under glycerine. Three to five fibers from two different samples were fractured in bending or tension, washed with water to remove the glycerine, and examined in the SEM after coating with gold. In many cases, both ends of a fiber were preserved so that mating fracture surfaces could be examined.

Typical SEM photos of fracture surfaces generated by breaking filaments in bending are shown in Figure 26. The origin of the fracture for the split fiber (Figure 26a) appears to be at the edges of the split. The fracture in the round fiber (Figure 26b) initiated at the surface of the fiber. Most of the fractures originated at the fiber surface and, in many cases, the fracture surface was not perpendicular to the fiber axis.

SEM photos of filaments broken under glycerine in tension are shown in Figures 27 and 28. The mating surfaces of the only filaments where fracture was initiated by a spherical inclusion are shown in Figure 27. Many pits are apparent on the surface of this filament in the region near the inclusion. The mating surfaces shown in Figure 28 are more typical of the majority of the fracture surfaces. The radial structure is evident, but there is no clear indication of fracture initiation by a surface flaw or an inclusion.
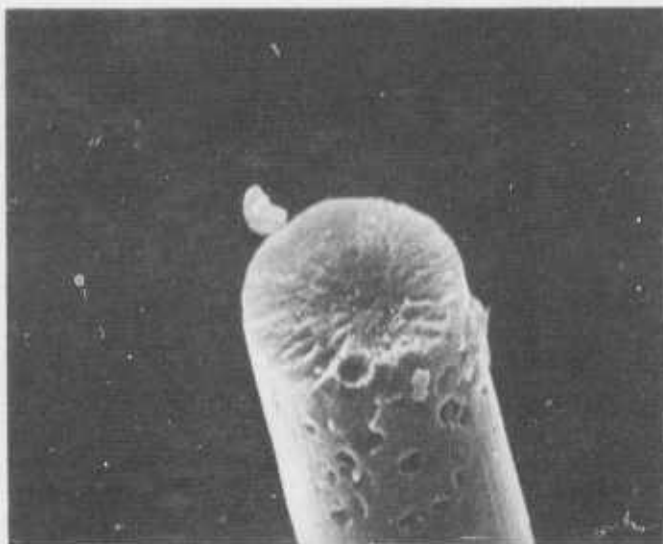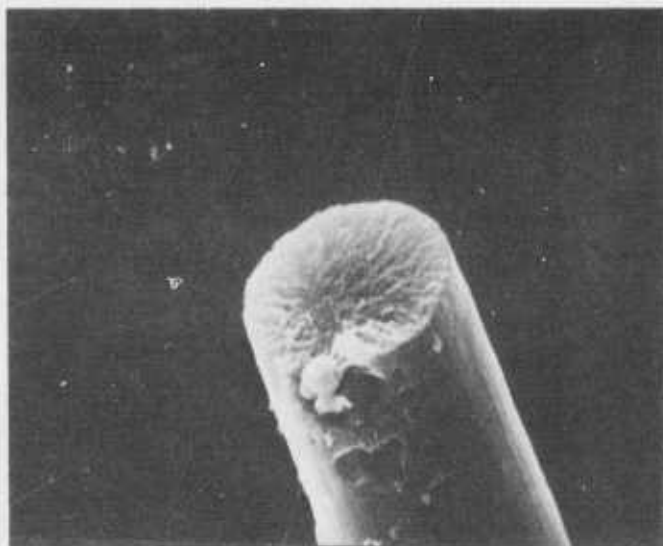
61
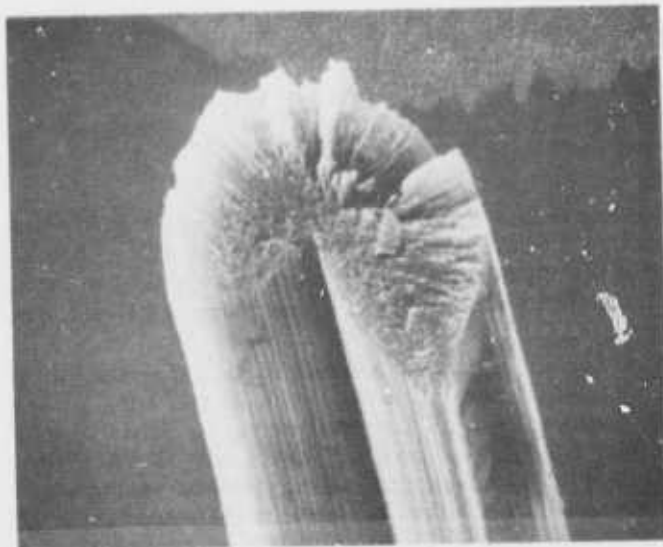
(a) 3000X
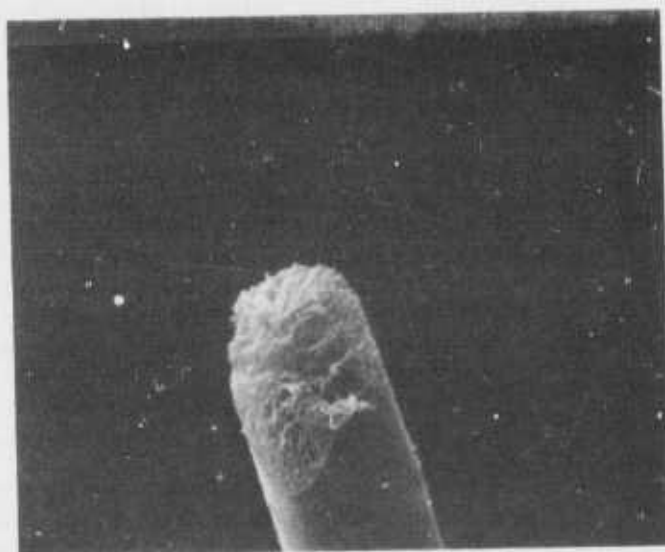
(b) 3500X

Figure 26. SEM Views of fibers fractured by bending under glycerine.
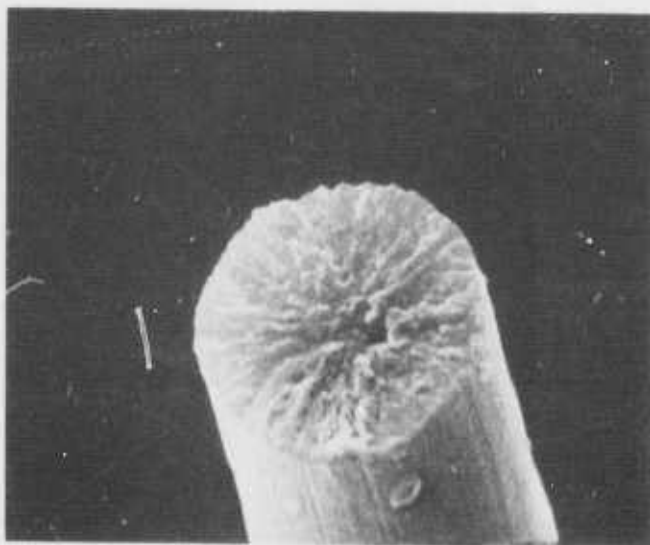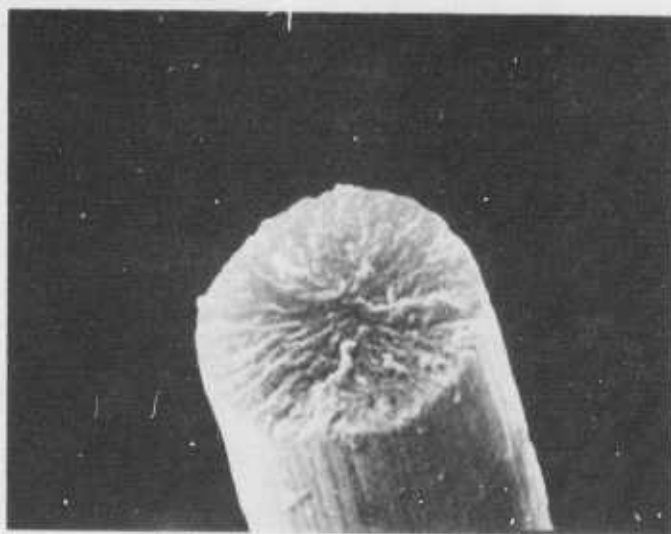
(a) 3500X

(b) 3500X

Figure 27. SEM views of the mating fracture surfaces
in a filament broken in tension under glycerine.

(a) 7000X

(b) 7000X

Figure 28. SEM views of the mating fracture surfaces
in a filament broken in tension under glycerine.

64

In contrast to bending fractures, the fracture surfaces for most of the filaments broken in tension were perpendicular to the fiber axis. The reason for these differences in fracture modes is not obvious, but fracture surfaces which are not perpendicular to the fiber axis as in Figure 26b, could occur as a result of variations in the degree of orientation in the particular area of the fiber.

Although the technique was not used extensively, the results obtained with breaking filaments under glycerine were quite successful. One can be reasonably certain that the original fracture surfaces have been preserved. The examination of mating surfaces helps considerably in verifying this assumption, and is useful in interpreting the features on the fracture surfaces. The latter advantage is evident in Figure 27 where an inclusion is visible on only one of the fracture surfaces.

SECTION VI

COMPOSITES WITH TYPE P FIBERS

With the increasing availability of larger quantities of experimental yarns from company funded programs, it became possible to test the performance of Type P fibers in composites. As mentioned in the previous reports of this series, the multifilament yarn produced at that time contained varying amounts of cracked filaments. Yarn with filaments free of cracks was obtained only rarely while yarn with completely cracked filaments was very common. In view of the results described in Section V of this report, it was deemed necessary to assess whether, and to what extent, the cracked filaments had a deleterious effect on the fiber performance in the composites.

1. Selection of Fibers

Yarns were selected according to their content of cracked filaments. Two batches (2-128 and 2-137) consisted of practically all cracked filaments. One batch (2-117) had approximately 25 percent of cracked filaments. Two remaining batches (2-107 and 2-139) were picked as examples of yarn with completely uncracked filaments. Unfortunately, after the composites had been manufactured and examined microscopically, it turned out that the yarn in one of the spools of the batch 2-139 contained predominantly cracked filaments. Consequently, approximately 15 percent of the filaments in the composite were present in that form.

At least 2000 meters of each 720 filament yarn were surface treated and wound up on six separate spools. Yarn on each spool was then strand-tested for the uniformity of strength and modulus and for the effectiveness of surface treatment. The results in Table XVII clearly demonstrate that these properties were quite uniform in each batch of fibers.

Fibers from batch 2-117 without surface treatment have been included in the test series to make sure that the composite properties reflected the improved shear strength in a normal fashion. Also, a set of test plates was prepared with standard surface treated "Thornel" 300 fibers as a check of the composite preparation and of the resin system performance. "Thornel" 50 fibers have been also included in the test series, because their interlaminar shear strength was expected to be closer to that of the Type P fibers. Unfortunately, "Thornel" 50 fibers did not respond to the available surface treatment which was used on all other fibers. The shear strength of the "Thornel" 50 fibers was, therefore, only 28.4 MPa, lowest of all fibers in the test series. Table XVIII presents the summary of the pertinent properties of all fibers used for making composites.

TABLE XVII

Uniformity Test of Type P Fibers Used in Making Composites

Batch No.		Tensile Strength GPa	Young's Modulus GPa	Torsional Shear MPa	Density Mg/m^3
2-117		1.39	228	72.4	1.99
		1.37	216	74.5	2.01
		1.39	231	70.3	2.01
		1.38	225	75.2	2.01
		1.34	237	62.7	2.00
		1.39	229	72.4	2.00
	Avg.	1.38	228	71.3	2.00
2-128		0.91	227	64.1	1.98
		0.85	235		2.01
		1.07	243		1.98
		0.92	241		1.99
		1.01	248		2.01
		0.94	245		2.01
	Avg.	0.95	240	64.1*	2.00
2-137		1.06	230	88.3	2.01
		1.00	230	80.7	2.01
		1.14	236	82.1	2.00
		1.13	231	84.1	1.99
		1.06	231	91.7	1.98
		1.25	241	90.3	2.02
	Avg.	1.11	233	86.2	2.00
2-139		1.41	248	82.1	2.00
		1.57	259	89.7	1.97
		1.65	238		
		1.55	290	79.3	1.97
		1.69	284	85.5	1.98
		1.52	287	84.1	1.99
		1.61	274	83.4	1.98
	Avg.	1.57	269	84.0	1.98
2-107		2.14	269	79.3	2.10
		1.99	241	91.7	1.99
		1.71	206	82.8	2.03
		2.09	262	93.8	1.99
		1.87	266	97.9	1.99
		2.08	285	92.4	2.07
	Avg.	1.97	225	89.7	2.03

* Not sufficient fiber to test each spool. The torsional test was performed on one rod prepared with an assemblage of fibers taken from all spools.

TABLE XVIII

Properties of Fibers Used in Composites

		Fiber Properties (Strand Test)			
Batch No.	Surface Treatment	d Mg/m^3	T.S.S. MPa	T.S. GPa	Y's M. GPa
T-300	yes	1.75	89.5	2.50	220
T-50	no	1.61	28.4	1.72	311
2-117	no	1.98	47.6	1.27	211
2-117	yes	2.00	71.3	1.38	229
2-128	yes	2.00	64.1	0.95	240
2-137	yes	2.00	86.2	1.11	233
2-139	yes	1.98	84.1	1.57	269
2-107	yes	2.03	89.7	1.97	255

2. Preparation of Composites

All fibers were wet-wound into prepreg using Resin 2544, a solvent-free proprietary high performance epoxy with very good shelf life and handleability. Sheets of prepreg were drum-wound, laid out flat, and cut to the desired size to make two plates with each yarn. All plates were cured in an autoclave for one hour at 95°C, for 1/2 an hour at 115°C, and for 8 hours at 165°C under a pressure of 90 psi. The plates earmarked for tensile tests were 250 mm long and about 1.5 mm thick. Plates intended to provide the short beam shear and the Texaco compressive test data had dimensions of at least 75 x 75 x 3 mm. Flexural test samples were cut from both types of plates since the thickness of the flex samples does not affect the test which is performed at a span-to-thickness ratio of 32:1 on 12.5 mm wide specimens. Resin contents and densities were obtained on every plate made. The micro-structure was examined on polished cross sections to make sure every plate tested was free of voids and delaminations.

3. Composite Properties

The results of all tests performed on composite plates are summarized in Table XIX. The numbers are averages of at least three tests. The properties of the "Thornel" 300 plates are in line with the results commonly obtained with these fibers indicating that both the composite preparation and the resin system were well controlled. The plate made with "Thornel" 50 fibers (no surface treatment) was the only one which clearly failed in compression during the flexural strength test, in keeping with its low Texaco compressive strength (T.C.S.) and very low interlaminar and short beam shear strengths (S.B.S.).

68

TABLE XIX

Composite Properties, as Measured, and Normalized to 60 Volume Percent Fiber Loading

Plate and Fiber Code	Fiber Vol. %	d Mg/m³	S.B.S. MPa	T.C.S. GPa	T.S. GPa	Flex. GPa	Y's M. GPa	S.M. GPa	T.S. GPa	Transl. %	Flex. GPa	Transl.(5) %	Y's M. GPa	Transl. %	cracked filam. in comp. (vol. %)
			Composite Properties, as measured						Normalized to 60 Vol. % fiber						
Thornel 300	62	1.57	99.4	1.10	1.43	1.57	135	115	1.38	92	1.48	99	130	99	0
Thornel 50(1)	55	1.45	18.1	0.40	0.89	0.70(a)	177	149	0.97	94	0.77	43	187	100	0
P2-117(1)	50	1.61	39.5(4)	0.43	0.45	0.54	110	91.1	0.54	71	0.65	85	132	100 -	25
P2-117	51	1.60	66.2(4)	0.47	0.74	0.70	111	84.4	0.87	96	0.82	100	131	95	25
P2-128	46	1.59	57.0(4)	0.42	0.43	0.38	109	84.6	0.56	100	0.50	87	156	100 -	> 95
P2-137	48	1.59	58.2	0.50	0.39	0.46	105	89.2	0.49	73	0.60(3)	90	132	95	~100
P2-139	57	1.64	71.0	0.56	0.65	0.76	142	125	0.68	72	0.81	85	149	91	10% mixed piles
P2-107	58	1.65	76.7	0.67	1.04	0.93	123	106	1.07	91	1.01	86	126	82	0

(1) Fibers without surface treatment.
(2) Failed in compression.
(3) Based on a plate with 46% fiber.
(4) Failed probably in compression without delamination
(5) Based on the tensile strength of fibers.

Composites P2-117 and P2-128 probably suffered a compressive failure during the short beam test, but clearly without delamination in spite of a 4:1 span to thickness ratio. The translation of the tensile strength of the Type P fibers is quite good for three out of five composites made with surface treated fibers. Composites P2-137 and P2-139, when normalized to 60 percent fiber loading utilizes less than 75 percent of the fiber strength. Whatever the reasons for this poor performance, they clearly are not related to the presence of the cracked filaments, because the composite P2-128 consisting of 100 percent cracked filaments shows 100 percent translation of the tensile properties. The balance between the tensile and flexural strengths is generally good, but the Texaco compressive strength is low. The experimental errors in the Texaco compressive tests are large, and a clear relationship with the content of cracked filaments cannot be established. Nevertheless, the composite P2-107 made with all uncracked filaments clearly has the highest compressive strength which represents 72 percent of the tensile strength vs. 77 percent in the "Thornel" 300 composite. In view of the low fiber loadings achieved in most Type P fiber plates, all above results must be viewed in the light of the structure of these composites.

4. Composite Structure

Figure 29 shows two polished sections of "Thornel" 300 plate, perpendicular to the fiber direction, at magnifications of 50X and 250X. A dense regular array of individual strands is clearly outlined by very thin layers of epoxy surrounding each strand. The fibers within each yarn bundle are distributed quite uniformly, approaching hexagonal close-packing with some vacancies, as can be seen from the photomicrograph at the higher magnification. Longitudinal "on-edge" view of the same composite at 100X magnification is shown in Figure 30. Excellent collimation of filaments is obvious. The resin rich region probably represents the boundary between two yarn bundles. The "Thornel" 50 plates looked very similar; lower fiber volume was reflected in considerably less dense packing of individual filaments within yarn bundles.

The composites made from Type P fibers were markedly different. Figure 31 shows the cross section of a plate made from the fiber 2-117 which had 25 percent cracked filaments. (The final content of cracked filament in the composite was actually obtained from a count of approximately 1000 filaments in a plate cross section at 250X magnification). Figure 31 reveals the presence of several very thick filaments. The individual strands in this composite are very loosely packed and separated by large islands of resin which appear also in the interior of the yarn bundles. Nevertheless, the normalized properties of this composite reflected an almost perfect translation of all pertinent properties of the fibers. Plates made with the fiber 2-128 (95 percent cracked) had a very similar appearance with slightly larger amounts of resin, as expected from its lower fiber loading. This composite exhibited the lowest flexural strength among all plates. Surprisingly, the composite made with the fiber 2-137 (100 percent cracked) with 48 percent fiber loading had a better fiber distribution than the previous plates with Type P fibers (Figure 32). Nevertheless, its properties were practically the same. A still better structure has developed in the composite made with 57 volume percent of the fiber 2-139 which consisted of predominantly round filaments (Figure 33).
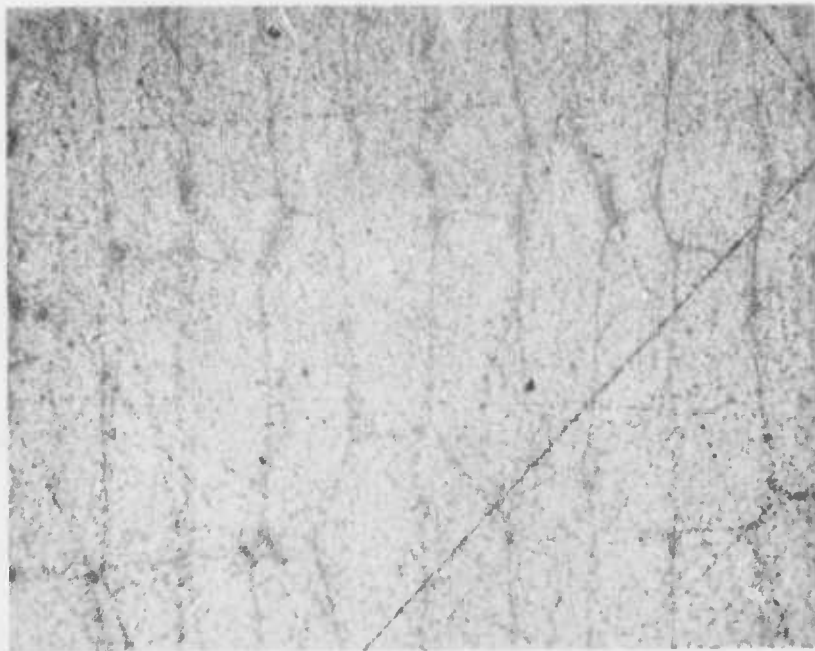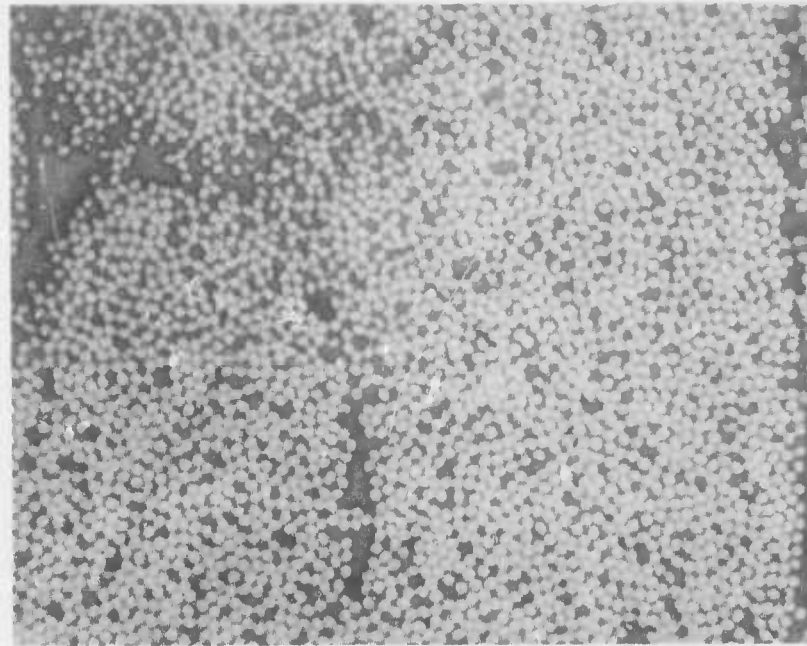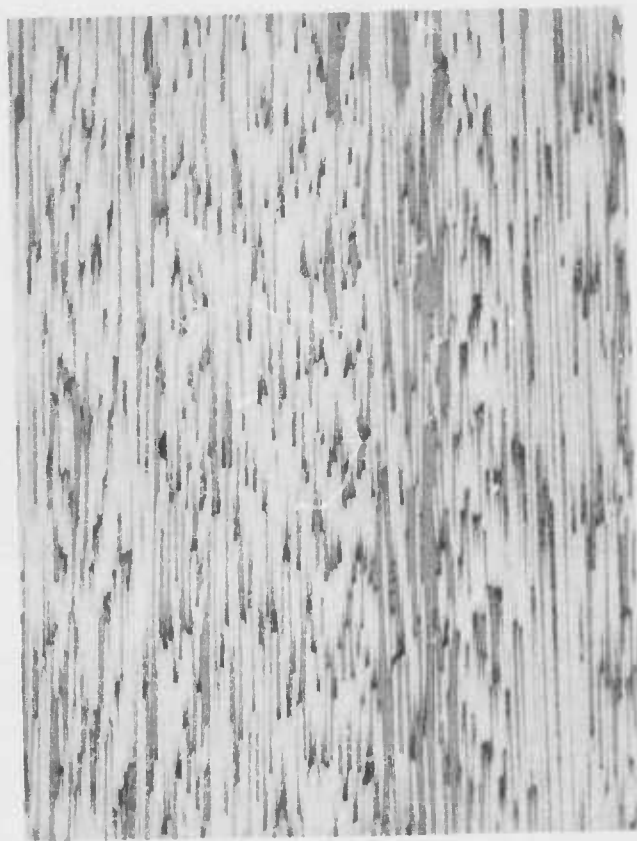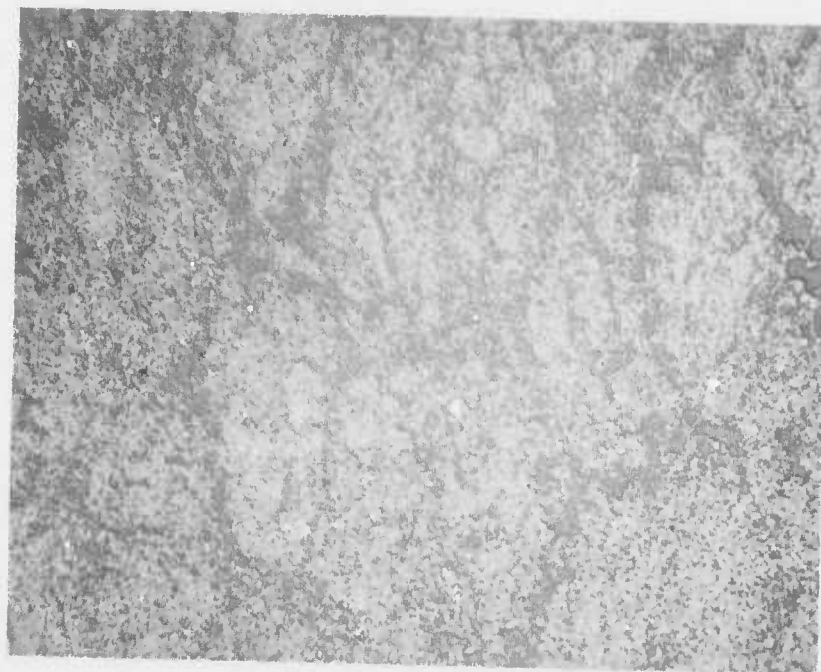
250X

50X
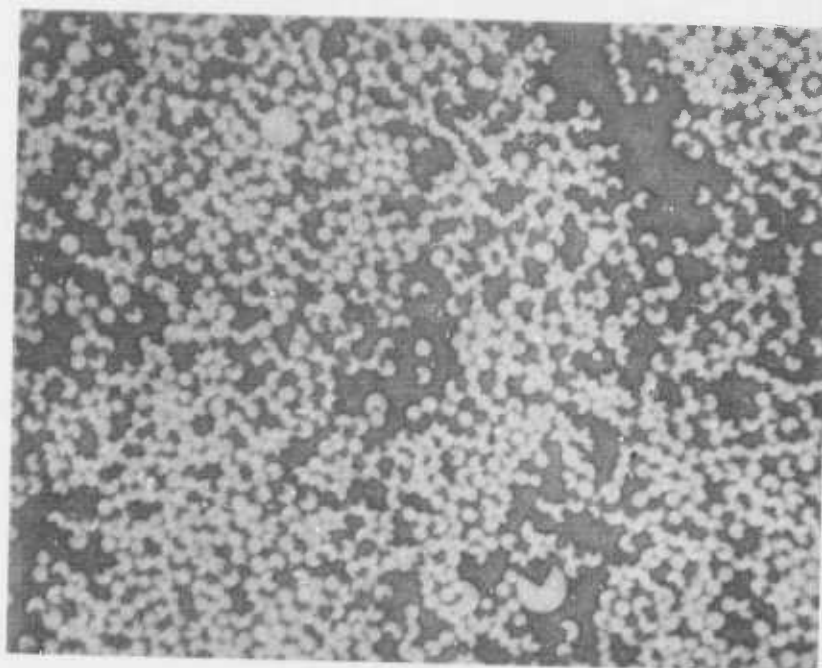
Figure 29. Cross sections of "Thornel" 300 composite.

100X

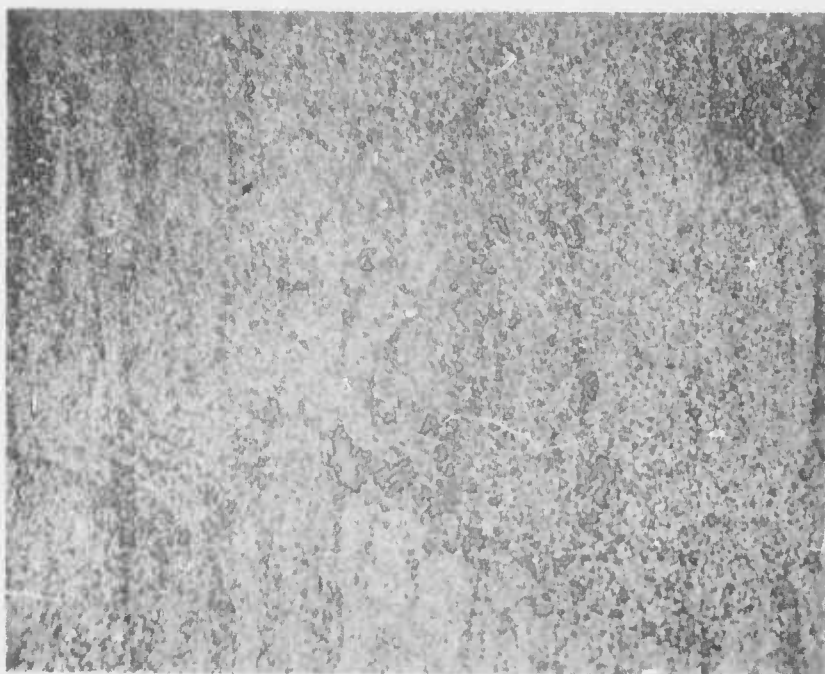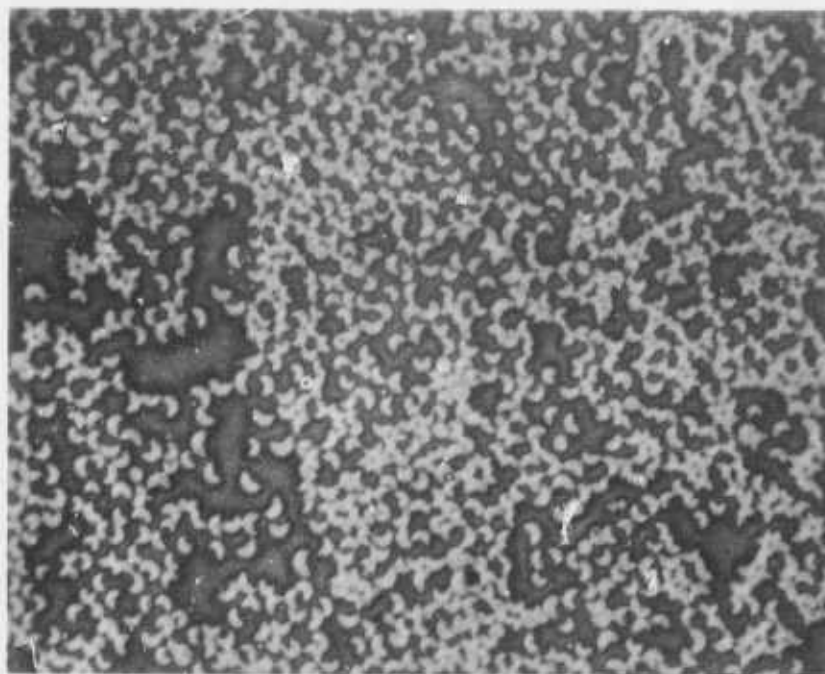Figure 30.   Longitudinal section of "Thornel" 300 composite.

250X

50X

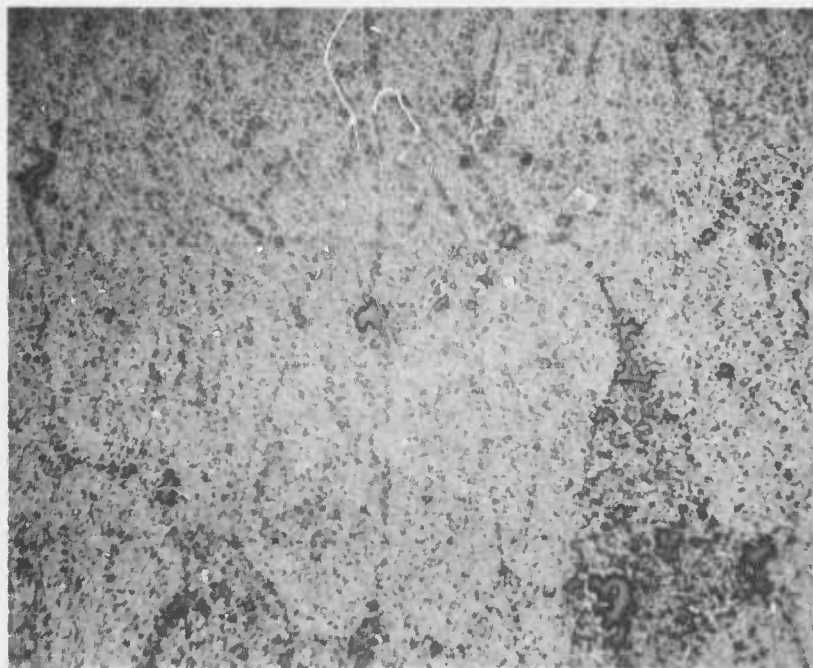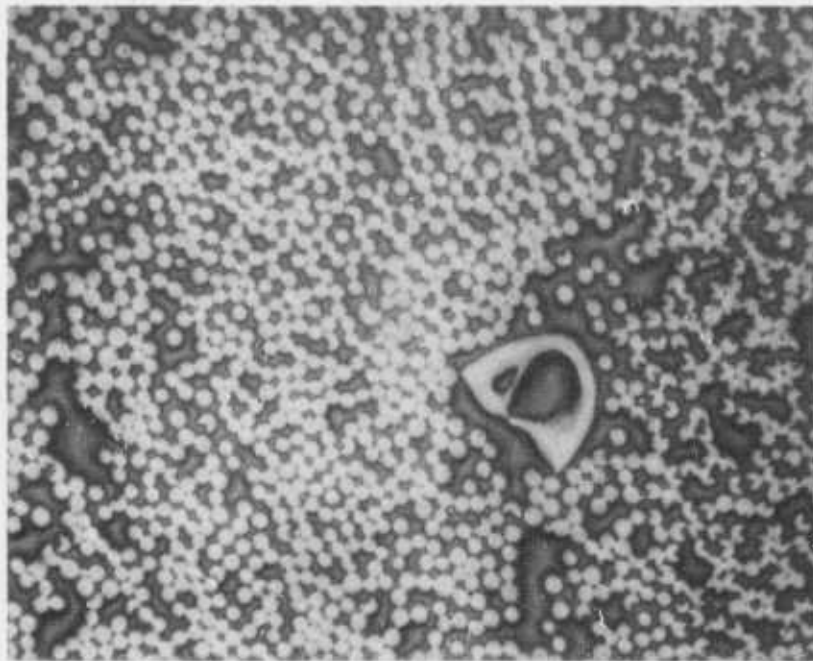Figure 31. Cross sections of Type P fiber composite (fiber batch 2-117).

250X

50X

Figure 32.   Cross section of Type P fiber composite (Fiber Batch 2-137)
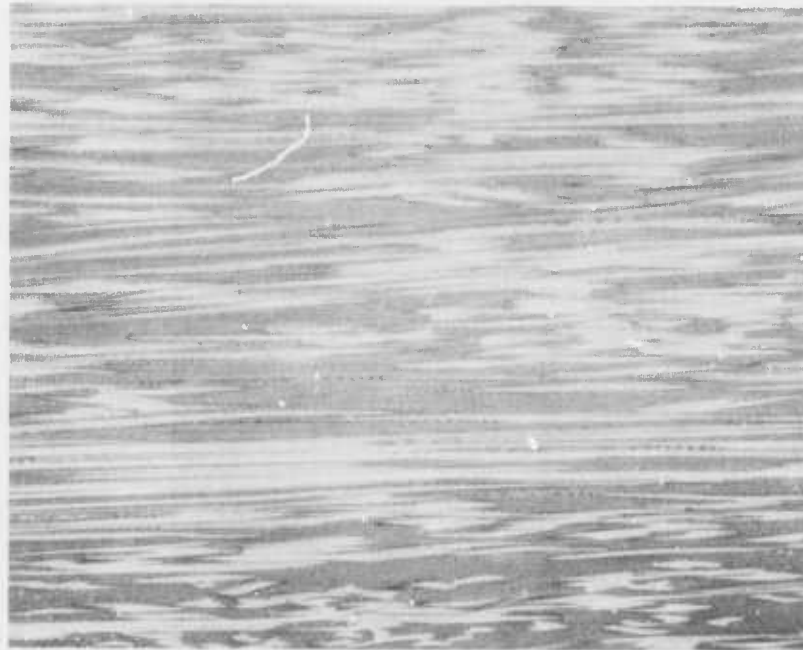
250X

50X

Figure 33. Cross sections of Type P fiber composite (Fiber Batch 2-139)

75

At the lower magnification, a fairly regular array of densely packed filament bundles can be seen. Some strands, however, had soaked up large amounts of resin and assumed a very irregular cross section. (See lower left corner of the photomicrograph at 50X.) The photomicrograph taken at higher magnification, clearly shows that these epoxy-rich strands consist of predominantly cracked filaments. One abnormally large structure in the lower part of this section is unique: it has not been observed in the remainder of the composite section. Polarized light photomicrographs of longitudinal sections (top and edge views) of the plates P2-137 and P2-139 revealed another undesirable feature of these composites: the filaments are poorly collimated, particularly in the plate 2-137 where a large number of filaments appear as oblique cross sections indicative of rope-like intertwining (Figure 34). The overall dark appearance of these photomicrographs is caused by the relatively high resin content in the composite. The filament alignment appears to be better in the plate 2-139, but several discrete areas showed a considerable amount of intertwined filaments (Figure 35). Most likely, these structural imperfections are to some extent responsible for the poor translation of fiber properties because only straight filaments carry the major portion of the load. Compressive strength, in particular, must be very sensitive to the presence of bent, twisted, and poorly collimated filaments; the buckling of filaments in the composites is commonly believed to be the dominant cause of compressive failure. Clearly then, no conclusions about the ultimate performance of Type P fibers in composites can be made until yarn with much better collimation becomes available.

This cautious stance is further reinforced by the structure of composite P2-107 which was made with best fibers and, consequently, gave the best properties. One may be tempted to attribute good performance of this composite to the fact that the fibers were all round. Perhaps equally important, however, was the structure of the composite itself. The cross section in Figure 36 is very reminiscent of that obtained with "Thornel" 300 fibers. Except for a somewhat higher resin content and less uniform filament packing, the edge view (Figure 37) exhibits a vertical alignment of the fibers that is much improved in comparison with the composites P2-137 and P2-139, but less perfect than the alignment in the T-300 composite. There is plenty of opportunity for nonuniform filament loading and, particularly, for fiber buckling that could account for the relatively low compressive strength of this composite and for the still incomplete translation of the tensile and elastic properties of the fibers.

5. SEM Fractography of Composites

The Scanning Electron Microscope is the best tool to investigate the fracture surfaces of composites. Tensile heat specimens of all composite plates were gold-plated and observed with a Scanning Electron Microscope at magnifications of 400X, 1000X and 1500X. Pictures were taken from most representative areas. Figure 38 shows the fracture surface of the "Thornel" 300 plate. A considerable amount of fiber pull-out occurred in spite of good torsional and short beam shear strengths, measured both on the fibers and on the composite (See Tables XVII and XIX). The mode of fracture of the tensile plate 2-107 was very similar in appearance, typical of well-behaved composites (Figure 39). The radial structure of the round filaments in the yarn 2-107 is very apparent at the higher magnification. Large regions of resin separating individual filaments are also clearly visible.
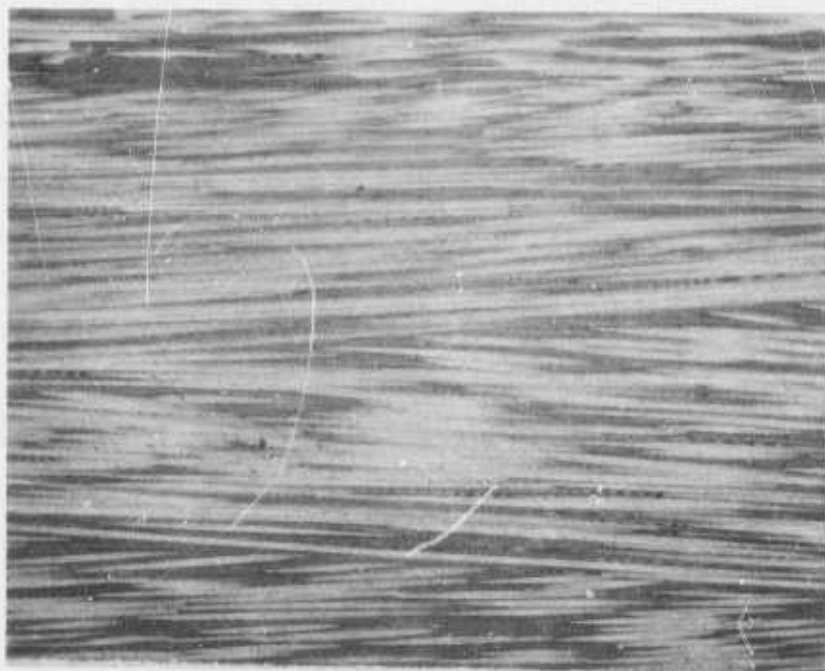
Edge
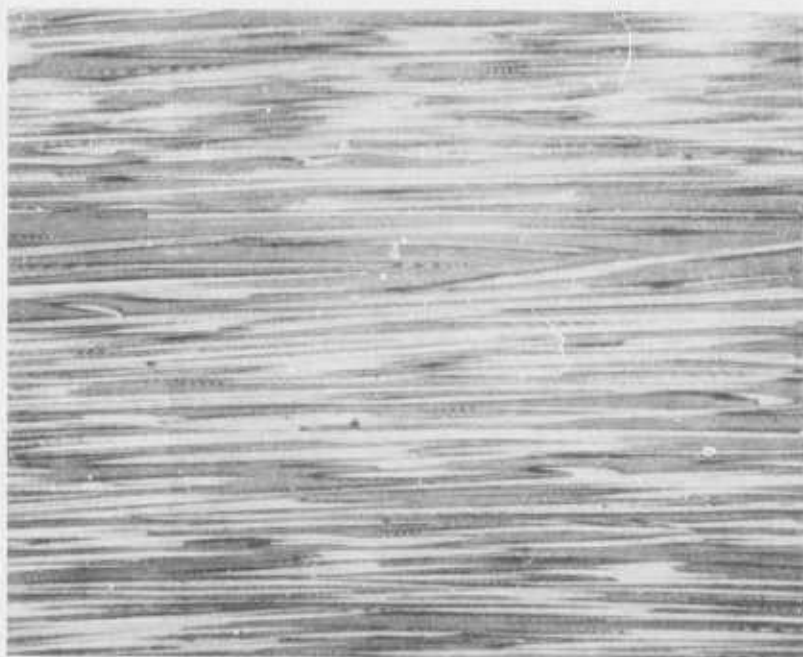
Top

Figure 34. Top and edge views of the composite plate 2-137 in polarized light (100X)
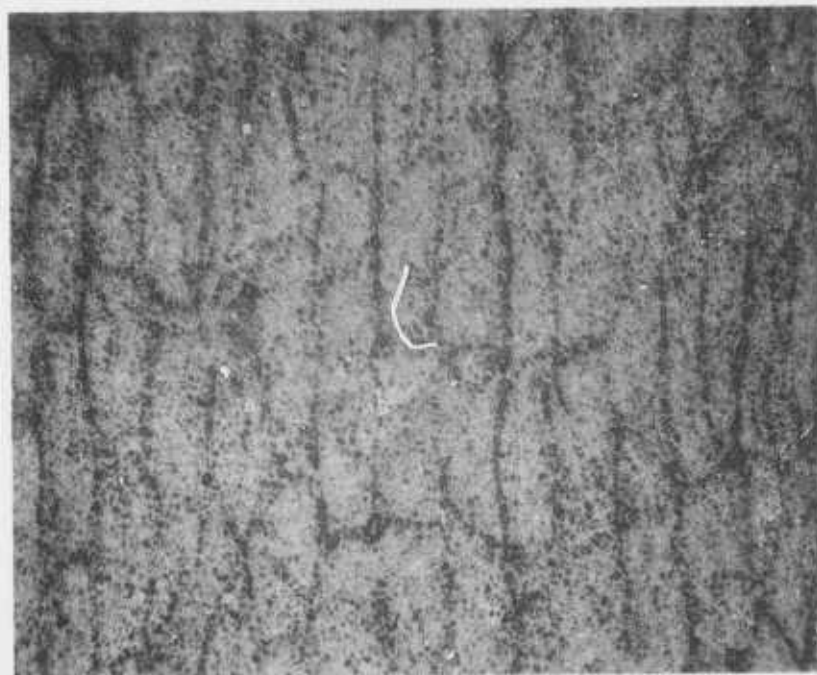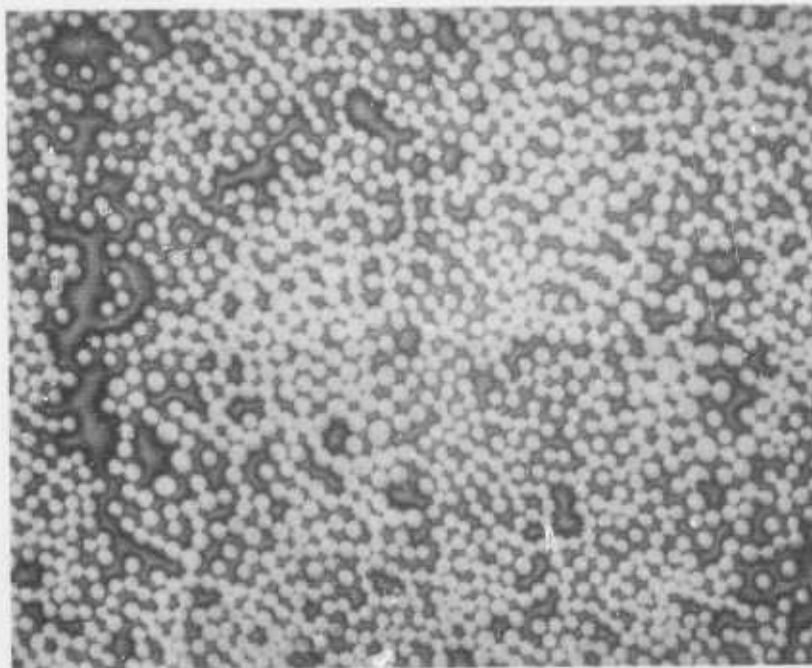
Top   Edge

Figure 35.   Top and edge view of the composite plate 2-139 (100X)

78

250X

50X

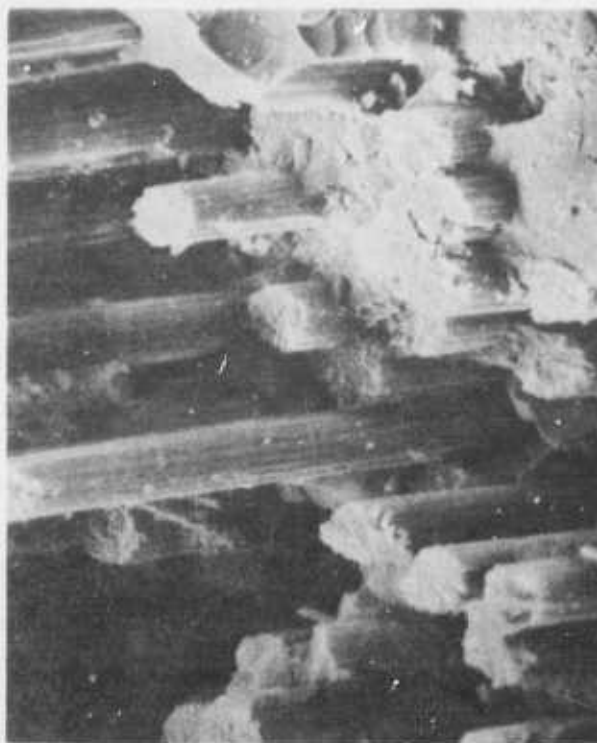Figure 36. Cross section of Type P fiber composite (Fiber Batch 2-107)

79

100X

Figure 37. Longitudinal section of Type P fiber composite (Fiber Batch 2-107)
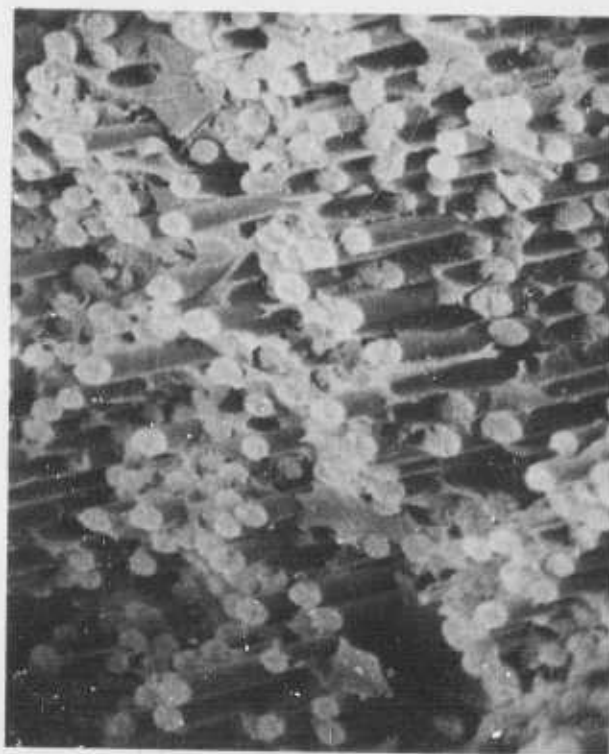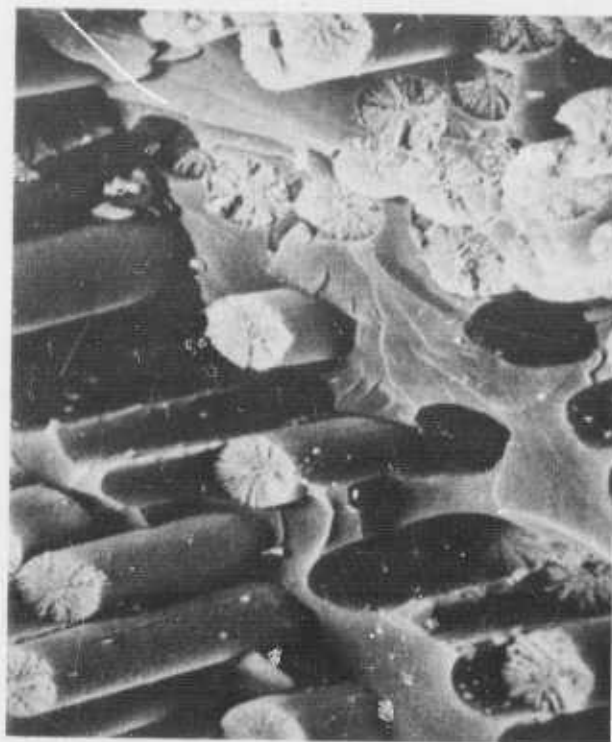
400X 1000X

Figure 38. Fracture surface of "Thornel" 300 composite observed
in SEM at 400X and 1000X magnification

400X   1000X

Figure 39. Fracture surface of P2-107 plate in SEM at 400X and
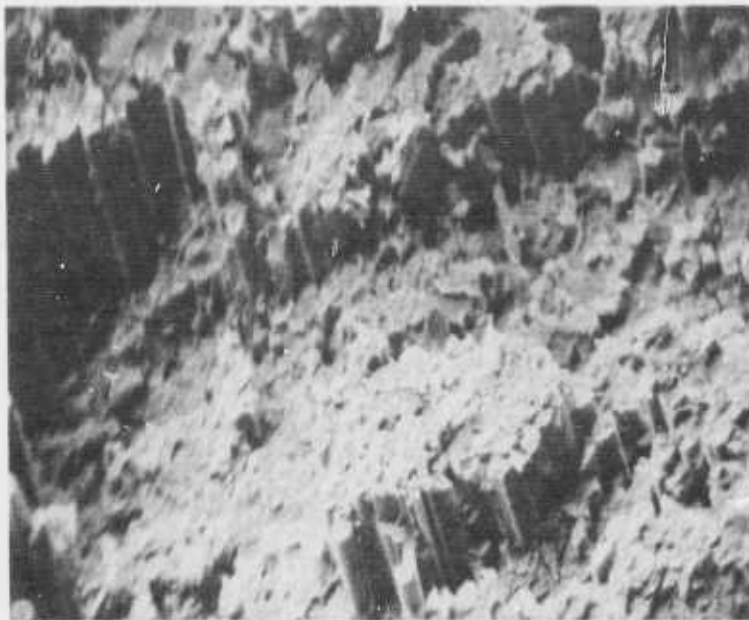1000X magnification

The fracture surfaces of all other composites with Type P fibers were very similar. Their only distinguishing feature, visible at low magnification, was the presence of numerous steps and exposed fiber bundles, as shown in Figure 40. The filaments exhibited very clean fracture surfaces without any evidence of shear failure which might be expected to occur in filaments with highly developed radial structures (See Figure 41).

All in all, SEM examination did not reveal any unusual features in the fracture behavior of the composites made with Type P fibers. Inadequate collimation of filaments in the yarn appears as the main deficiency of Type P fibers at their present state of development. Poor collimation is particularly pronounced in fibers that contain large amounts of cracked filament because the crack is associated with spiral distortion of the filaments (See Section V-4). As a result, the filaments are loosely packed and the achievable fiber loading of composites is low. Furthermore, uneven fiber loading and fiber buckling are very likely to occur, resulting in incomplete translation of tensile properties and in low compressive strength. Well collimated fibers can be expected to show much improved performance.

6. Strands Made with Monofilament Tow

Several attempts were made to test the properties of the monofilaments in epoxy-resin impregnated strands which, for all practical purposes, represent "mini-composites." For this purpose, monofilament was spun from ultrafiltered pitch into several bands containing 1000 - 1200 filaments each. The bands were then cut and separated from the spool as short tows of about 300 mm length. The fibers were processed to 1700°C. Without surface treatments, the properties of the filaments were nearly identical to those described in Section III-2 of this report. (Long gauge T.S. - 2.50 GPa, short gauge T.S. - 3.2 GPa, Young's modulus 210 GPa.) The fibers were impregnated with epoxy by pulling the tow through a liquid resin bath. A weighted clip was attached to one end of each strand and the "mini-composites" were cured under tension in an oven. It was apparent during all steps of the processing and impregnation that some filaments broke while others were becoming tangled. In spite of most careful handling, it was not possible to eliminate such damage.

The monofilament strands were subjected to standard yarn testing and evaluation, i.e., the results were obtained as fiber properties calculated on the basis of the total area of filaments in the strand which is derived from the weight of fibers and their density. The results are shown in Table XX. As usual, the translation of the Young's modulus was very good, but the strength of the strand filaments was only 60 percent of the single filament strength. This discrepancy cannot be attributed to any gauge length effects because the shortest strand was the weakest. Moreover, previous tests with Type P yarn strands showed that there was no dependence on the gauge length in the range between 25 and 250 mm. Again, one is compelled to blame the low apparent tensile strength of the monofilament in the strand on the lack of collimation caused by entanglement during processing. It is known that relatively small amounts of misorientation can have a disastrous effect on the strength of fiber reinforced composites.[14]

83

400X

Figure 40. Fracture surface of composite plate P2-117
in SEM at 400X magnification
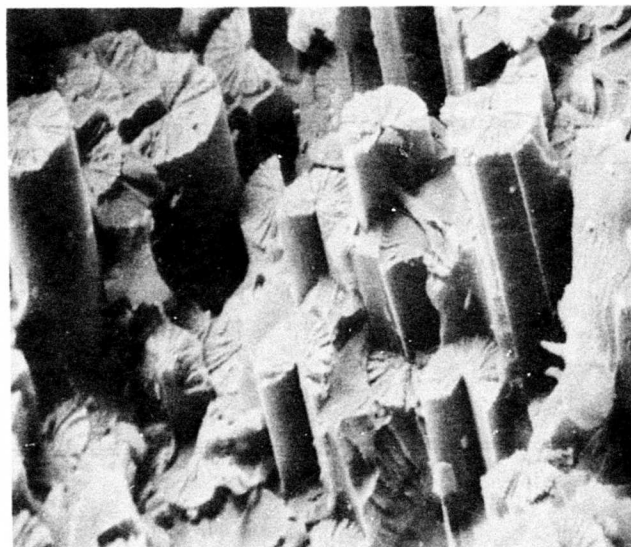
1000X

Figure 41. Fracture surface of composite plate P2-128 in
SEM at 1000X magnification

TABLE XX

Strand Tests of Monofilament Tow

Strand	Test Gauge Length, cm	Tensile Strength GPa	Kpsi	Young's modulus GPa	Mpsi
1	12.7	1.99	288	227	33
2	12.7	1.89	275	232	34
3	12.7	1.44	209	204	30
4	7.6	1.36	197	211	31

REFERENCES

1 T. Araki, K. Asano and T. Kurio, Jap. Patent 40093 - 1972, Oct. 1972.

2 T. Araki, K. Asano, H. Takita and T. Aivao, U. S. Patent 3,718,574, February, 1973.

3 B. J. Wicks and R. A. Coyle, J. Mat. Sci., 11, 376, 1976.

4 Union Carbide Corporation, "Graphite Fibers from Pitch," Technical Report AFML-TR-73-147, Part I, June 1973, p. 34.

5 A. G. Metcalfe and G. K. Schmitz, Proceedings Amer. Soc. Test. Mat. 64, 1075, 1964.

6 Union Carbide Corporation, "Graphite Fibers from Pitch," Technical Report AFML-TR-73-147, Part III, p. 16.

7 D. Robson, F.Y.I. Assabghy, E. G. Cooper and D. J. E. Ingram, J. Phys. D: Applied Phys. 6, 1822, 1973.

8 Union Carbide Corporation, "Graphite Fibers from Pitch," Technical Report AFML-TR-73-147, Part II, March 1974, p. 58.

9 Union Carbide Corporation, "Graphite Fibers from Pitch," Technical Report AFML-TR-73-147, Part III, July 1975, p. 44.

10 C. D. Hain, R. R. Lamonte and Y. T. Shah, J. Appl. Poly. Sci., 16, 3307, 1972.

11 L. W. Davis and P. G. Sullivan, American Ceramic Society Bulletin, September 1974, Abstract 2-CM-74P.

12 Union Carbide Corporation, "Graphite Fibers from Pitch," Technical Report AFML-TR-73-1974, Part II, p. 33.

13 J. E. Zimmer, J. L. White, J. S. Evangelide, and R. A. Meyer, The Aerospace Corporation. "Re-entry Vehicles Materials Technology." Report No. TOR-0076 (6726-02) - 2, Vol. I, September 1975.

14 A. Kelly, "Strong Solids", Clarendon Press, Oxford, 1973, p. 218.